

Mads Mehus Ivarson

Numerical study of flow calming structures in hydropower plants

Master's thesis in Mechanical Engineering
June 2021

NTNU
Norwegian University of Science and Technology
Faculty of Engineering
Department of Energy and Process Engineering

Mads Mehus Ivarson

Numerical study of flow calming structures in hydropower plants

Master's thesis in Mechanical Engineering
June 2021

Norwegian University of Science and Technology
Faculty of Engineering
Department of Energy and Process Engineering



NTNU

Kunnskap for en bedre verden

Master`s Agreement / Main Thesis Agreement

Faculty	Faculty of Engineering
Institute	Department of Energy and Process Engineering
Programme Code	MTPROD
Course Code	TEP4925

Personal Information	
Surname, First Name	Ivarson, Mads Mehus
Date of Birth	29.12.1995
Email	madsmi@stud.ntnu.no

Supervision and Co-authors	
Supervisor	Chirag Trivedi
Co-supervisors (if applicable)	Kaspar Vereide, Pål-Tore Selbo Storli
Co-authors (if applicable)	

The Master`s thesis	
Starting Date	15.01.2021
Submission Deadline	11.06.2021
Thesis Working Title	Numerical Study of Flow Calming Structures in Hydropower Plants
Problem Description	<p>Several large hydropower plants in Norway have been upgraded with a higher installed capacity, however, this has resulted in certain operational challenges associated with sediments entering the penstock and causing wear to the hydro turbine. One of the reasons may be a limitation in the sand trap that may not function as anticipated after the refurbishment. A test-case of sand trap available from 960 MW Tonstad (Sira-Kvina) hydropower plants expected to investigate. Work in master thesis is built upon the project work conducted during Autumn 2020. Student has conducted computational fluid dynamic (CFD) and verified the numerical model. The previous work focused on testing of different methodologies including isolated and coupled multiphase flow simulations. Coupled multiphase flow simulation results found realistic and physically correct. However, those are preliminary results. Work under the master thesis will aim to obtain robust and credible solution using CFD and validate with the experimental data (if available in the</p>

	<p>repository). The work will include more complexities, such as wall roughness, accurate inlet velocity profile and extending the model to capture the entire sand trap. The quantification of the effects of the flow calming structure on the trap efficiency of the sandtrap should be carried out. The thesis work may either focus on detailed study of the FCS-design, Sira-Kvina have been working with so far, or there can be comparison study of two different types. 1. The following tasks are to be considered The main tasks are related to numerical modelling of flow through intake systems, specifically sand traps, and determine the head losses and efficiency. The project work is part of tasks proposed by Sira-Kvina kraftselskap on CFD modelling of sand trap system and continuing the previous project work. All activities are built upon project work conducted during Autumn 2020. Following tasks are expected to carry out for master thesis work.</p> <ul style="list-style-type: none"> □ Preparing a robust numerical model of the intake system, focus should be hexahedral mesh high quality discretization of the domain and more accurate boundary conditions. □ Current method of determining the head losses and the sand trap efficiency is not robust enough. Investigate the robust method for determining the sand trap efficiency and the head losses. □ Furthermore, the rib section in the downstream end should be included, to ensure that a certain amount of the sediments is trapped. Then it will be possible to assess the change in trap efficiency with and without the flow calming structures. □ □ Investigate the fluid mechanic aspect of generation of turbulence, breakdown of turbulent structure, particle trajectory. Because initial hypothesis was, for the flow calming structure, to breakdown the large turbulent structure, and ultimately reducing the time before the turbulence from the inlet section is dissipated. □ Upon completion of the master thesis work, data shall be submitted to the repository in the Waterpower Laboratory along with the filled forms of data management plan.
--	--

Preface

This work was conducted at the Waterpower Laboratory, Norwegian University of Science and Technology (NTNU) in the spring of 2021. Associate professor Chirag Trivedi from NTNU and Dr. Kaspar Vereide from Sira-Kvina power company have been supervisors for this thesis.

Abstract

In order to increase the life span of hydraulic turbines in hydropower plants, it is necessary to minimize damages caused by sediment erosion. One solution is to reduce the amount of sediments by improving the sand trap. In the present work, the effects on sand trap efficiency by installing v-shaped rake structures for flow distribution and rib structures for sediment trapping is investigated numerically using the SAS-SST turbulence model. Three-dimensional models of the sand trap in Tonstad hydropower plant are created. The v-shaped rake structures are located in the diffuser near the inlet of the sand trap, while the ribs cover a section of the bed in the downstream end. The present study showed that when including ribs in the model, the total weight of sediments escaping the sand trap is reduced by 24.5 % from the base value. This leads to an improved sand trap efficiency. Consequently, the head losses in the sand trap are increased by 1.8 %. By including the v-shaped rakes in addition, the total weight of sediments escaping the sand trap is instead increased by 48.5 % from the base value, thus worsening the sand trap efficiency. This increases head losses by 12.7 %. The results also show that turbulent flow commencing at the sand trap diffuser prevents the downstream settling of sediments with a diameter of < 1 mm. The hydraulic representation of the numerical model is validated by comparing to PIV measurements of the flow field from scale experiments and ADCP measurements from the prototype.

This master thesis is paper based. The research paper is submitted to the journal Energies, on 01 June 2021 and it is under review as of 11 June 2021 (thesis submission date).

Ivarson, MM., Trivedi, C., and Vereide, K., 2021, "Investigations of rake and rib type structures in sand traps to prevent sediment transport in hydropower plants," submitted to journal, Energies, on 01 June 2021, manuscript id energies-1265138.

Sammendrag

For å forlenge livsløpet til hydrauliske turbiner er det nødvendig å minimere skader forårsaket av sedimentslitasje. En mulig løsning er å forbedre sandfanget for å redusere mengden sedimenter som når turbinene. I dette arbeidet brukes numeriske simuleringer til å undersøke hvordan installering av v-formede raker ved sandfangets innløp og ribber ved utløpet påvirker sandfangseffektiviteten. Det har blitt laget tre-dimensjonelle modeller av sandfanget i Tonstad kraftverk. Arbeidet viser at inkludering av ribber reduserer den totale sedimentmassen som forlater sandfanget med 24.5 % fra basisverdien, noe som leder til økt sandfangseffektivitet. Som en konsekvens øker sandfangets falltap med 1.8 %. Inkludering av de v-formede rakene i tillegg øker heller den totale sedimentmassen som forlater sandfanget med 48.5 % fra basisverdien. Dermed synker sandfangseffektiviteten. Dette øker også falltaptet med 12.7 %. Resultatene viser også at turbulente strømminger som oppstår i diffuseren gjør at sedimenter med diameter mindre enn 1 mm forhindres i å slå seg til ro i sandfanget. Den hydrauliske representasjonen av den numeriske modellen valideres ved å sammenligne med PIV-målinger av strømningsfeltet i skalaeksperimenter og med ADCP-målinger fra det faktiske sandfanget.

Denne masteroppgaven er også skrevet som en artikkel. Artikkelen er innlevert til journalen Energies den 01 juni 2021 og er under vurdering per 11 juni 2021 (innleveringsfrist for masteroppgave).

Ivarson, MM., Trivedi, C., and Vereide, K., 2021, "Investigations of rake and rib type structures in sand traps to prevent sediment transport in hydropower plants," innlevert til journal, Energies, den 01 June 2021, manuskript-id energies-1265138.

Acknowledgements

I would like to express my sincere gratitude to my supervisor Associate Professor Chirag Trivedi, who has tirelessly provided guidance and answered my questions during this work. I am grateful towards my co-supervisor Dr. Kaspar Vereide for valuable input and interesting discussions, and for the opportunity to work on such an interesting research project.

I would like to thank all the people at the Waterpower Laboratory for the conversations, wine lotteries and ping pong matches. These have kept me motivated throughout this project, and have made the days at the lab much brighter.

I am thankful to Dr. Wolfgang Richter at Graz University of Technology, Austria for providing data to validate the numerical model.

Finally I want to thank my girlfriend and family for always cheering me on and listening to my both my joys and frustrations during my years at NTNU. You have been there to support me when I have needed it and I am very lucky to have you with me.

Contents

Preface	i
Abstract	iii
Sammendrag	v
Acknowledgments	vii
Contents	ix
List of Tables	xi
List of Figures	xv
Nomenclature	xvii
1 Introduction	1
2 Theory and methods	5
2.1 Sediment transport theory	5
2.2 Head loss	6

2.3	Turbulence modelling	7
2.4	Computational setup	9
2.4.1	Geometry and mesh	9
2.4.2	Solution parameters	12
2.4.3	Multiphase	13
2.4.4	Mesh independence study	15
3	Results and discussions	17
3.1	Sand trap efficiency	17
3.2	Head losses	18
3.3	Model 1: No upgrades	19
3.4	Model 2: Sand trap with ribs	21
3.5	Model 3: Sand trap with v-shaped rakes and ribs	23
3.6	Particle tracks	25
4	Conclusion	29
	References	31
A	Appendix – A	35

List of Tables

2.1	Mesh quality parameters.	11
2.2	Transient simulation solution parameters.	13
2.3	Parameters in mesh independence study.	16
3.1	Sand trap efficiencies	18
3.2	Head loss, Δh_L , is calculated using Equation 2.3. Increased head loss is found by comparing to model with no upgrades.	19

List of Figures

1.1	Location of Tonstad power plant marked in red.	2
1.2	Layout of a typical high-head hydropower plant. The sand trap is circled in red.	3
2.1	Types of sediment transport.	6
2.2	a) The sand trap without upgrades. The distance from end of diffuser to the weir is 184 m. The diffuser is 16 m long. The sand trap tunnel has a cross-sectional area of 119 m ² . b) Ribs. The ribs are placed just upstream of the penstock, and are 1 m wide and spaced apart by 1 m. The ramp has an 8 % inclination. c) Top view of the v-shaped rakes in the diffuser. The v-shaped rakes measure 6 m in height. Distances tip-to-tip between rakes are 1 m and 0.8 m for the upstream and downstream row, respectively. Zoomed part shows rake dimensions.	10
2.3	Mesh near the ribs.	12
3.1	Velocity distributions in the sand trap with no upgrades included at t = 1000 s. A high velocity jet above vortices caused by flow separation can be seen in the diffuser. Further downstream, the velocity is more evenly distributed.	20

3.2	Sand trap without upgrades, symmetry plane at $t = 1000$ s. a) Velocity contour. Flow separation occurs in the diffuser which causes a higher flow velocity in the upper part of the diffuser. Separation is also seen to occur at the weir. b) Vorticity contour. Flow separation in the diffuser and at the weir causes vortex generation. c) Turbulence kinetic energy contour. Turbulence propagating from the diffuser starts to dissipate before reaching the penstock.	20
3.3	View of the sand trap on the symmetry plane at $t = 1000$ s. a) Velocity contour. A separated flow field can be observed over and under the ribs. Flow is identical to the model with no upgrades up until the ramp and ribs. b) Vorticity contour. c) Turbulence kinetic energy contour. Higher turbulence flow is seen to enter the penstock.	21
3.4	Zoomed view of ribs in the symmetry plane at $t = 1000$ s. a) Velocity contour. b) Vorticity contour. c) Turbulence kinetic energy contour.	22
3.5	Sand trap with ribs and v-shaped rakes, symmetry plane at $t = 1000$ s. a) Velocity contour. Flow over the rakes is accelerated, while flow going through the rakes slows down and turns turbulent. b) Vorticity contour. High vorticity appears immediately downstream of rakes and remains throughout the sand trap. c) Turbulence kinetic energy contour. Rakes induce higher levels of turbulence than can be seen in models without rakes. Turbulence has not dissipated before the flow exits the sand trap.	24
3.6	Zoomed view of v-shaped rakes in symmetry and horizontal planes at $t = 1000$ s. a) Velocity contours. b) Vorticity contours. c) Turbulence kinetic energy contours.	25
3.7	Particle track plot at ribs without v-shaped rakes in the diffuser. Only particles smaller than 1 mm remain suspended when reaching the ribs. These are gathered low in the sand trap. Bed load sediments pour between the ribs.	26
3.8	Particle track plot at ribs with v-shaped rakes in the diffuser. Sediments are more dispersed over the tunnel cross-section. Larger amounts of sediments are suspended in the flow and pass the ribs.	26
A.1	Engineering drawing of the Tonstad power plant sand trap.[Ref: Sira-Kvina kraftselskap, (2020)]	35

A.2	Engineering drawing of the Tonstad power plant sand trap. Parts of the drawing has been removed, by Sira-Kvina's request.[Ref: Sira-Kvina kraftselskap, (2020)]	36
-----	---	----

Nomenclature

Abbreviation

CFD Computational fluid dynamics

DPM Discrete phase model

NTNU Norwegian University of Science and Technology

Symbols

D Diameter (m)

F Force (N)

f Darcy friction factor (-)

g Gravitational acceleration (m/s^2)

h_f Friction head loss (m)

L Length (m)

p Pressure (Pa)

Re Reynolds number (-)

t Time (s)

U Mean flow velocity (m/s)

u' Velocity fluctuations (m/s)

u^* Flow shear velocity (m/s)

v	Flow velocity (m/s)
w	Sedimentation velocity (m/s)

Greek symbols

δ	Kronecker delta function
ϵ	Turbulent kinetic energy dissipation rate (m^2/s^3)
η	Sand trap efficiency
k	Turbulent kinetic energy (m^2/s^2)
ν_T	Turbulent viscosity (m^2/s)
ω	Turbulent kinetic energy dissipation (1/s)
ρ	Density (kg/m^3)

Chapter 1

Introduction

Sediment handling and erosion in hydropower plants are long-standing engineering challenges. Hydropower plants are often upgraded and refurbished to improve performance and plant capacity. After upgrading their installed capacity, several large Norwegian hydropower plants have experienced operational problems associated with sediments entering the penstock and causing erosion to the turbine [1]. Moreover, a higher variability in power demand in recent years has led to some plants converting from base-load to peak-load production. This results in variable discharge through the tunnels, which stirs up sediments from the tunnel bed in unlined tunnels with remaining rock material on the invert, which is typical in Norwegian hydropower plants.

Tonstad hydropower plant, located in the mountains of south-western Norway, is currently experiencing such challenges. In 1988, the plant upgraded its capacity from 640 to 960 MW by installing a third 320 MW Francis turbine. An additional penstock, surge tank, and sand trap was built. However, the unlined headrace tunnel was left untouched. It was expected that the higher discharge required to run all three turbines would lead to an increased amount of sand and rocks to be flushed into the turbines. However, the actual amount of sediments being transported with the flow was surprisingly large. One of the reasons for the increased amount of sediment transport is the poor design of the sand trap, which was designed in the 1960s, and is now under-performing.

Figure 1.2 shows the layout of a typical high-head hydropower plant. A sand trap is a section of the water way, typically located immediately upstream of the penstock. This allows the headrace tunnel, with remaining stone and sand material after its construction, to be unlined. Sand traps are designed to reduce flow velocity, which allows sediments to settle easier. The velocity is typically reduced by 30 to 50 % [1]. This is done by increasing the cross-sectional area of the tunnel. The main



Figure 1.1: Location of Tonstad power plant marked in red.

challenge is the poor performance of sand trap, which is supposed to trap sediments before they reach the penstock. A proposal to improve sand trap performance is to cover sections of the bed with concrete ribs. This has been shown in physical experiments to create a low velocity zone beneath the ribs, protecting sediments on the bed from being stirred up, while also allowing sediments to fall through the gaps between ribs [2, 3]. Another proposal is to install rows of v-shaped rakes in the diffuser at the sand trap inlet. Increased levels of turbulence, such as those induced by these v-shaped rakes, has been shown to increase sediment settling speeds for certain particle sizes in numerical studies by Maxey in 1987 [4] and Wang & Maxey in 1993 [5]. This was later confirmed in physical experiments by Aliseda et al. in 2002 [6]. In these studies, sediments were found to settle in the peripheries of local vortex structures, which is coupled to a sweeping of sediments in directions normal to the flow.

Several scientific studies have been conducted on the topic of sediment transport in hydropower sand traps. Olsen & Skoglund modelled the flow of water and sediment in a three-dimensional sand trap geometry using the $k - \epsilon$ turbulence model [7]. After including modifications to the turbulence model, both the flow field solution and sediment concentration calculations were in agreement with experimental procedures. Kjellesvig & Olsen modelled the bed changes in a sand trap using the transient convection-diffusion equation for sediment concentration and an adaptive grid adjusting for changes in the bed [8]. Large amounts of sediments could be seen being moved through the geometry in the simulations. The results compared well to physical model tests. Bråtveit & Olsen used 3D computational fluid dynamics (CFD) simulations to calibrate horizontal acoustic Doppler current profilers (H-ADCP) in the Tonstad sand trap [9]. The study found that the 3D CFD simulations

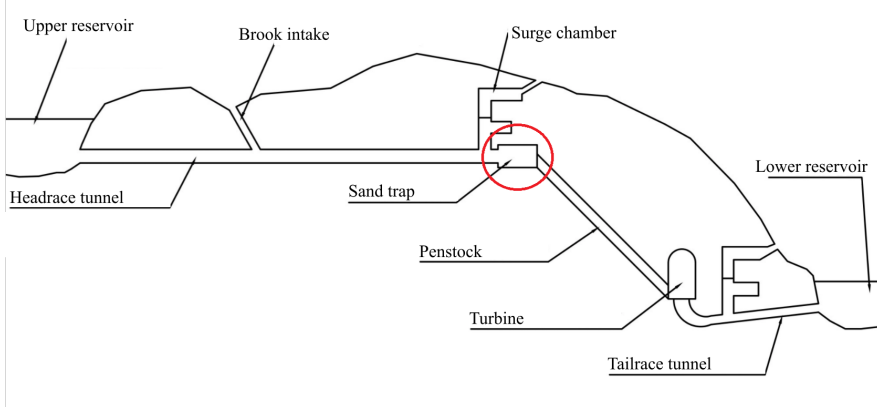


Figure 1.2: Layout of a typical high-head hydropower plant. The sand trap is circled in red.

could accurately calibrate the H-ADCP, while also assessing the flow conditions at the locations of installation. Almeland et al. computed water flow in a model of the Tonstad sand trap using different versions of the $k - \epsilon$ turbulence model [10]. Depending on the discretization scheme, grid resolution and turbulence model, the computations showed the flow field to follow both the left side, right side and center of the diffuser. Field measurements showed that the main current follows the center of the diffuser.

The present work is a part of an ongoing sand trap research project. In previous work, it has been found that implementing ribs just upstream of the penstock increased sand trap efficiency dramatically, as sediments were trapped in the low velocity zone underneath the ribs [2, 3]. Havrevoll et al. performed PIV analyses on the flow around ribs in the sand trap to investigate the sediment settling characteristics. They show that the ribs successfully separate the flow field [11]. Daxnerova performed experiments on a physical scale model of the sand trap at NTNU to determine the effects of installing various flow calming structure designs in the diffuser [12]. The best performing design from Daxnerova's research, a v-shaped rake type structure, will be further studied in this work.

The objectives of the present work is to assess the changes in sand trap efficiency by including ribs in the downstream end of the sand trap. The effects on the turbulence dissipation and sediment trajectories by including v-shaped rakes in the diffuser will be investigated. The work aims to reproduce results from experiments on physical scale models of the sand trap in order to gain further confidence in the experimental results.

Chapter 2

Theory and methods

The concepts, equations and methods presented in this section lay the theoretical foundation for the simulations. They are vital in order to understand how results were obtained and how they were interpreted.

2.1 Sediment transport theory

When sediments at the tunnel bed are subjected to shear stresses higher than what is required to loosen them from the bed, they will be suspended and transported with the flow. Sediment transport can be divided into two main categories, depending on the shear velocity to settling velocity ratio of the particles, $u^* > w$ [13]. These categories are *suspended load* and *bed load*. Suspended load consists of finer particles which have low inertia and settling velocities due to their low mass. They are therefore transported further by the flow before settling, compared to bed load sediments. The bed load usually consists of rocks and larger grains of sand which are too heavy to be suspended in water for longer durations. They are instead transported by sliding, saltating or rolling along the sediment bed, as illustrated in Figure 2.1.

In order to determine if the upgrades improve sediment settling, it is necessary to measure the sand trap efficiency. The most straight-forward method to compute the efficiency is a sediment mass based approach. Here, the ratio of total mass of sediments injected at the inlet and escaped through the outlet is found. The efficiency can then be calculated as in Equation 2.1

$$\eta = 1 - \frac{\Phi_{s,out}}{\Phi_{s,in}} \quad (2.1)$$

where, η is the sand trap efficiency and Φ represents the mass of sediment. Time

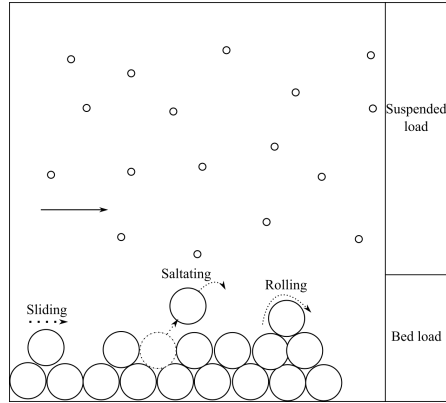


Figure 2.1: Types of sediment transport.

integrated particle mass flow reports created at the end of simulations will be used to find the inflow and outflow of sediments for calculating the sand trap efficiencies.

2.2 Head loss

Installing new structures in the waterways could increase the energy losses in the flow. This is mainly due to increased friction. This will affect the total head loss and ultimately the performance of the power plant. The head loss should therefore be minimized. Losses due to friction are determined by using the Darcy-Weisbach friction factor, seen in Equation 2.2.

$$h_f = f \frac{L \times v^2}{D \times 2g} \quad (2.2)$$

Here, h_f (m) is the head loss, f is the dimensionless Darcy friction factor, L (m) is the length of the pipe, v (m/s) is the mean velocity of the flow, D (m) is the diameter of the tunnel, g (m/s²) is the gravitational acceleration. To ensure correct head loss calculations, it is important to find the correct Darcy friction factor. Using a Moody diagram, the friction factor can be found from knowing the Reynolds number and relative roughness of the flow situation. In the present work, the Darcy-Weisbach equation form based on the pressure drop (Equation 2.3) will be used to find the head loss caused by the upgrades.

$$\Delta h_L = \frac{\Delta p}{\rho g} \quad (2.3)$$

Here, Δh_L is the head loss, Δp (Pa) is the pressure difference between two points, and ρ (kg/m^3) is the fluid density. The head loss in each of the geometries will be measured in post-processing. The head loss in the base case will be subtracted from each of the other cases, where the difference is the increased head loss caused by the upgrades.

2.3 Turbulence modelling

Due to its chaotic and unpredictable nature, turbulence can only be solved directly for a few simple flow cases. In order to predict the effects of turbulence, one can use Reynolds decomposition on the continuity and momentum equations, before time-averaging the results[14]. This will give the RANS equations.

$$U_j \frac{\partial U_i}{\partial x_j} = \frac{1}{\rho} \frac{\partial}{\partial x_j} (-P\delta_{ij} + 2\mu S_{ij} - \overline{\rho u'_i u'_j}) \quad (2.4)$$

where $S_{ij} = \frac{1}{2}(\frac{\partial U_i}{\partial x_j} + \frac{\partial U_j}{\partial x_i})$ (1/s) is the mean strain rate, δ_{ij} is the dimensionless Kronecker delta function and $\overline{\rho u'_i u'_j}$ (N/m^2) is the Reynolds stress term. As can be observed, the RANS equations give rise to the fluctuating Reynolds stress term, which behaves like a physical stress term on the mean flow. The unknowns contained in the Reynolds stress term need to be modelled as a function of the mean flow in order to remove any fluctuating parts of the equations.

The two most common two-equation turbulence models are k - ω and k - ϵ . The latter is mostly used to simulate mean flow characteristics of a turbulent flow. It attempts to predict turbulence by solving two PDEs for the turbulent kinetic energy, k and the rate of turbulent energy dissipation, ϵ . The k - ϵ model is given in Equation 2.5 and Equation 2.6.

$$\frac{\partial k}{\partial t} + U_j \frac{\partial k}{\partial x_j} = \frac{\partial}{\partial x_j} \left[\frac{\nu_T}{\sigma_k} \frac{\partial k}{\partial x_j} \right] + P_k - \epsilon \quad (2.5)$$

$$\frac{\partial \epsilon}{\partial t} + U_j \frac{\partial \epsilon}{\partial x_j} = \frac{\partial}{\partial x_j} \left[\frac{\nu_T}{\sigma_\epsilon} \frac{\partial \epsilon}{\partial x_j} \right] + \frac{\epsilon}{k} (C_{e1} P_k - C_{e2} \epsilon) \quad (2.6)$$

where

$$P_k = 2\nu_T S_{ij} \frac{\partial U_i}{\partial x_j}, \nu_T = C_\mu \frac{k^2}{\epsilon} \quad (2.7)$$

and σ_k , σ_ϵ , C_{e1} , C_{e2} and C_{mu} are empirical constants[15].

The k - ω model solves the set of equations using the specific rate of turbulent kinetic energy dissipation, ω instead of ϵ . The model does well in predicting turbulent behaviour close to walls.

The k - ω model equations are given in Equation 2.8 and Equation 2.9.

$$\frac{\rho \partial k}{\partial t} + \frac{\partial \rho u_j k}{\partial x_j} = P - \beta^* \rho \omega k + \frac{\partial}{\partial x_j} \left[\left(\nu + \sigma_k \frac{\rho k}{\omega} \right) \frac{\partial k}{\partial_j} \right] \quad (2.8)$$

$$\frac{\rho \partial \omega}{\partial t} + \frac{\partial \rho u_j \omega}{\partial x_j} = \frac{\gamma \omega}{k} P - \beta \rho \omega^2 + \frac{\partial}{\partial x_j} \left[\left(\nu + \sigma_\omega \frac{\rho k}{\omega} \right) \frac{\partial \omega}{\partial_j} \right] \quad (2.9)$$

where

$$P = \tau_{ij} \frac{\partial u_i}{\partial x_j} \quad (2.10)$$

and β^* , β , γ , σ_k and σ_ω are constants[16].

A third option, the *Shear Stress Transport* k - ω , combines the k - ω and k - ϵ models by using the k - ω formulation close to the walls and a model similar to k - ϵ in the free-stream [16]. This makes the model directly usable down to the wall through the viscous sub-layer, while avoiding the common k - ω problem that the model is too sensitive to the inlet free-stream turbulence properties.

To model the turbulent flow behaviour in the present work, the scale-adaptive simulation shear stress transport (SAS-SST) turbulence model was used. The model was found to perform better than the conventional RANS formulations in similar cases during the under-lying project work. It introduces the von Karman length scale into the turbulence scale equation to adapt to different turbulence structure sizes, while using base RANS equations in areas where the flow behaves more similar to steady state[17]. The SAS-SST equations are as follows.

$$\frac{\partial k}{\partial t} + \frac{\partial u_j k}{\partial x_j} = P_k - \beta^* \omega k + \frac{\partial}{\partial x_j} \left[\left(\nu + \frac{\nu_t}{\sigma_k} \right) \frac{\partial k}{\partial x_j} \right] \quad (2.11)$$

$$\frac{\partial \omega}{\partial t} + \frac{\partial}{\partial x_j} (\bar{u}_j \omega) = \frac{\partial}{\partial x_j} \left[\left(\nu + \frac{\nu_t}{\sigma_\omega} \right) \frac{\partial \omega}{\partial x_j} \right] - \beta \omega^2 + C_\omega + \alpha S^2 (1 + P_{SAS}) \quad (2.12)$$

$$\nu_t \propto \frac{k}{\omega}, \quad P_{SAS} = \bar{\zeta}_2 \kappa \frac{L}{L_{vK,3D}}, \quad L_{vK,3D} = \kappa \frac{S}{U''} \quad (2.13)$$

In these equations, S and U'' are generic first and second velocity derivatives, respectively. The SAS-SST model builds on the SST k - ω model by implementing an extra production term in the ω -equation, P_{SAS} . This term is attuned

to transient fluctuations in the flow. In regions with a fine mesh where the flow is turning unsteady, $L_{vK,3D}$ is reduced, increasing the production term. This will result in a large ω and therefore reduced k and ν_t values. In this way, the unsteadiness is not dampened, but instead it is included as a part of the turbulence that is being resolved, leading to greater accuracy. A reduction of the turbulent viscosity dissipation happens, which makes the momentum equations interpret the flow as transient rather than steady[18].

2.4 Computational setup

2.4.1 Geometry and mesh

Advances in CFD in recent years have made it possible to extend the use of CFD to a wide range of complex engineering challenges. CFD uses numerical solution methods to analyze fluid flows, and provides cheaper and faster results compared to physical model experiments. In addition, CFD allows the study of large or dangerous systems, which is one of its unique advantages. However, there are several limitations and challenges when it comes to CFD modelling. Seeing as CFD modelling involves assumptions, simplifications and discretizations, these introduce errors and deviations from reality. It is also a tool which requires large computational resources, in the form of memory, CPU power and storage. These limit the time and space resolution of the solution, and a compromise between resolution and simulation time is necessary.

The Tonstad power plant sand trap is 184 m long and the main tunnel has a cross-sectional area of 119 m². A 3D model of the sand trap is developed using engineering CAD software. It was created from engineering drawings provided by Sira-Kvina power company, the owner of the plant, and consists of a rectangular inlet section, a diffuser, a long tunnel section with a gentle slope, and a weir in the invert where the tunnel transitions into the penstock. This model is used as a base to add the upgrades to in two other models. The additional models were created to test the effects of the upgrades, where one model includes only ribs and one includes both ribs and v-shaped rakes.

The ribs are placed just upstream of the penstock, in combination with the weir. This setup was tested in experiments [2, 3]. The purpose of the ribs is to allow bed load sediments to fall between the ribs, while only minimally affecting the flow of water. There are five ribs in total. The length of the ribs and the gap between each rib are both 1 m. A ramp is placed upstream of the ribs to raise them above the bed and create space for sediments to accumulate. Also, in this way, excavating into the tunnel floor is not necessary. In the work by Richter et al, the ramp was also found to protect the sediments that had fallen between the ribs from being resuspended

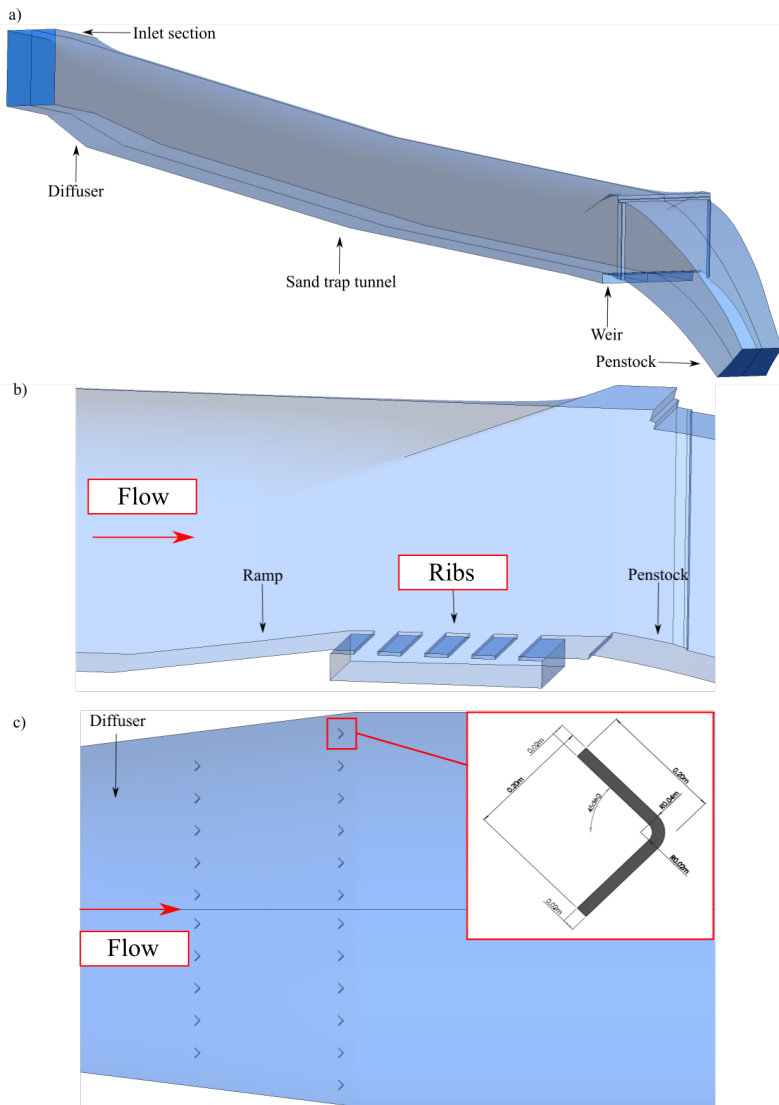


Figure 2.2: a) The sand trap without upgrades. The distance from end of diffuser to the weir is 184 m. The diffuser is 16 m long. The sand trap tunnel has a cross-sectional area of 119 m^2 . b) Ribs. The ribs are placed just upstream of the penstock, and are 1 m wide and spaced apart by 1 m. The ramp has an 8 % inclination. c) Top view of the v-shaped rakes in the diffuser. The v-shaped rakes measure 6 m in height. Distances tip-to-tip between rakes are 1 m and 0.8 m for the upstream and downstream row, respectively. Zoomed part shows rake dimensions.

Table 2.1: Mesh quality parameters.

Parameter	Description
Orthogonality	How close the angle between adjacent cell faces is to the optimal angle. The optimal angle for tetrahedral mesh structure is 60° .
Aspect ratio	Measure of the stretching of a cell, defined as the ratio between width and height.
Expansion ratio	How fast the cell sizes grow or shrink in a direction. Should not exceed 1.2 between cells.
Skewness ratio	How close the shape of a cell is to the ideal cell. Skewed elements may decrease accuracy and cause unstable solutions. Ratio ranges from 0 to 1, where 0 is the ideal cell.

and flushed into the penstock.

The rake structure is made up of two rows of v-shaped rakes, with the tip of the rakes facing downstream. The rakes measure 6 m in height. Distances between rakes are 1 m and 0.8 m for the upstream and downstream row, respectively. The purpose of the rakes is to even the flow of the jet from the inlet and enhance the diffuser effect of slowing down the flow. The distance from the inlet to the rakes is 25 meters, which is approximately 3 times the diameter. To ensure that stable and developed flow reaches the rakes, a distance of 5-10 times the inlet diameter is desired. The fact that the flow reaching the rakes may not be fully developed in the simulations should be taken into consideration when analysing the results.

Meshing is the discretization of the fluid domain, and divides the domain into smaller cells. The numerical equations are then applied to each cell. Together, they create a representation of the flow behaviour. The accuracy and convergence of the solution depends on the number of cells in the mesh. A coarse mesh will represent a more simplified version of the fluid domain than a fine mesh, and could result in higher discretization errors. There are several mesh parameters which can be monitored in order to ensure that a mesh is of sufficient quality. These parameters and their descriptions are listed in Table 2.1.

A mesh cell can have several different shapes. Different shapes have different purposes, depending on the problem at hand, desired accuracy of the solution and solver used. A mesh consisting of structured hexahedral cells typically offers shorter simulation times compared to other mesh types. Hexahedral meshes are generally more time consuming to create and have to be created manually when using Ansys Mesher. Tetrahedral meshes are appropriate for complex geometries,

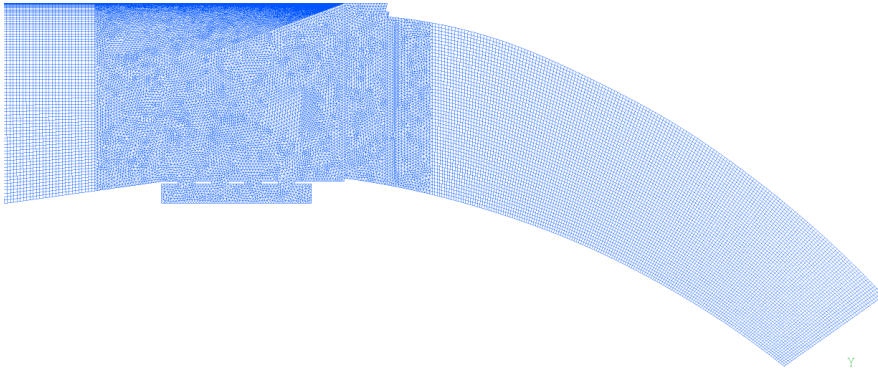


Figure 2.3: Mesh near the ribs.

where setting up a structured hexahedral mesh is deemed too difficult or time consuming.

The three geometrical models are meshed similarly. In all models, the diffuser and the invert are both given tetrahedral mesh structures, while the simpler geometries of the inlet section, tunnel and penstock have structured hexahedral meshes. The number of cells in each mesh is $> 23 \times 10^6$. Inflation layers are added along the tunnel walls so that global $Y^+ < 30$. This ensures accurate representation of flow conditions in the boundary layers. The mesh surrounding the ribs and the rakes are refined further to a maximum cell size of 0.01 m.

2.4.2 Solution parameters

The chosen advection scheme is the High Resolution scheme available in CFX. This scheme is second order accurate in smooth regions and reduces its order of accuracy in regions of high gradients, where unboundedness is a factor. A first order accurate scheme is generally more robust and reaches convergence criteria faster than a second order accurate scheme. However, this comes at the cost of higher numerical diffusion, resulting in a less accurate solution. The transient scheme used is the Second Order Backward Euler scheme.

Steady state multiphase simulations are run to create initial conditions for the transient simulations. The total simulated time for the transient simulations is set to allow sediments enough time to either reach the bed or exit through the outlet. The simulations use a discharge of $80 \text{ m}^3/\text{s}$, which is the discharge when the power plant is operating at design conditions. The inlet velocity boundary condition reflects this mass flow rate. The wall roughness is 10^{-3} m in the numerical model. An overview

Table 2.2: Transient simulation solution parameters.

Parameters	Description
Mesh type	Structured hexahedral and unstructured tetrahedral.
Model scale	1:1 to prototype.
Analysis type	Transient: total time of 1000 s, time step of 0.5 s.
Fluid	Incompressible Newtonian fluid, water density and viscosity at 10 C
Boundary conditions	Inlet: uniform velocity of 1.14 m/s. Outlet: total pressure of 0 Pa. Symmetry plane along center line.
Wall roughness	0.001 m.
Multiphase settings	Multiphase model: Discrete phase model/Particle transport solid. Fluid pair model: One-way coupled. Sediment mass flow rate: 1000 kg/s. Sediment particle diameter: $D_{particle} \sim N(0.75 \text{ mm}, 0.25 \text{ mm})$
Solver controls	Advection scheme: High Resolution. Transient scheme: Second Order Backward Euler.
Turbulence model	SAS-SST.
Convergence control	Maximum residuals for pressure, mass-momentum and turbulent parameters $< 10^{-4}$. Coefficient loops: 2-3 iterations.

of solution parameters and boundary conditions is presented in Table 2.2.

2.4.3 Multiphase

Multiphase flow was implemented by enabling the particle transport solid model in CFX, also known as the discrete phase model (DPM). DPM uses the Eulerian-Lagrangian multiphase model to track the paths of individual particles as they travel through the domain. It is well-suited for situations like in the present work, where the volume fraction of the solid phase is low. In the underlying project work, the Eulerian-Eulerian multiphase model was used. Instead of tracking individual particles, this model calculates the volume fraction of fluid to sediment in each cell. This is useful for monitoring settling locations, but makes it difficult to track particle trajectories when the relative sediment mass flow is low. It is also difficult to differentiate between large and small particles, which is one of the factors which are important to the results of the present work. The change to the DPM was therefore justified.

To solve the particle-fluid interactions in CFX, two models are available. The fully coupled fluid pair model is the most accurate one, and calculates the forces from each phase on the other. This model is also the most computationally expensive. In the one-way coupled fluid pair model, only the forces from the fluid phase acting on the solid phase are calculated. As a result, the model is computationally cheaper, but the solution will be simplified. However, in cases where the solid phase volume fraction is low and the forces from the solid phase on the fluid phase are negligible, this model yields comparable results to the fully coupled fluid pair model. To verify this, test simulations were run to compare the results from the two models. Here, the results from the one-way coupled model and the fully coupled model were identical. Because of this, the one-way coupled fluid pair model was used in the present work.

Choosing an adequate number of positions (NPP) representing particles in the domain is an important part of multiphase analyses. A larger NOP requires longer computation times and could dramatically increase the size of the simulation result file. The massflow rate of particles determines how many particles are represented by each position. For steady state simulations, the NOP should be proportional to the total number of particles injected into the domain. In the present study, NOP for steady state simulations was set to 2000. For transient simulations, the NOP should be proportional to the influx of particles each second. The number is therefore usually lower than for steady state because of computational limitations. NOP was set to 25 for the transient simulations.

Another set of important settings for multiphase simulations in CFX are the particle solver control settings. Here, you can define the particle tracking time, distance and iterations. For larger cases, the default values may not be sufficient in order to provide useful results. Therefore, some of these settings have to be modified. For the present work, the particle tracking time was set to 1000 s, which is the same as the simulated time for the transient simulations. This means that every particle injected into the domain will be tracked until the simulation is finished, unless it exits through the outlet. In addition, the particle tracking distance was set to 300 meters, which is slightly larger than the length of the model. A fitting number of particle iterations found by trial and error in test simulations, and was eventually set to 10^6 . The remaining particle solver control settings were left at their default values.

In the transient multiphase simulations, sediments were injected with uniform distribution over the inlet during the first 100 s. Mass flow of sediments is set to 1000 kg/s, which leads to a total mass of sediments injected into the sand trap to be 10^5 kg. The sediments are tracked as they travel through the model, and the in- and outflow of sediments are given by the time integrated mass flow report at the end

of the simulation. The sediment diameters have a normal distribution with a mean of 0.75 mm and a standard deviation of 0.25 mm.

2.4.4 Mesh independence study

By also ensuring that the solution is mesh independent, the accuracy of the results are further improved. Mesh independence is achieved when a defining value for the simulation no longer changes significantly with increasing mesh quality. The purpose of a mesh independence study is to minimize the discretization error from approximating the geometry during the meshing stage [19]. The model with both v-shaped rakes and ribs was used for the mesh independence study. Three different mesh qualities were used. Following the procedure described by Celik et al. [20], an estimation of the discretization error was performed. The mesh discretization error was found to be 1.4 %. The procedure for calculating the discretization error is as follows.

$$p = \frac{1}{\ln(r_{21})} \times |\ln |\epsilon_{32}|$$

$$\epsilon_{21} | + q(p)| \quad (2.14)$$

$$q(p) = \ln \frac{r_{21}^p - s}{r_{32}^p - s}, s = 1 \times \text{sgn}\left(\frac{\epsilon_{32}}{\epsilon_{21}}\right) \quad (2.15)$$

where $\epsilon_{32} = \phi_3 - \phi_2$, $\epsilon_{21} = \phi_2 - \phi_1$.

Afterwards, the extrapolated values were calculated using Equation 2.16.

$$\phi_{ext}^{21} = \frac{r_{21}^p \phi_1 - \phi_2}{r_{21}^p - 1} \quad (2.16)$$

ϕ_{ext}^{32} was similarly calculated.

The approximate and extrapolated relative errors were found using Equation 2.17 and Equation 2.18, respectively.

$$e_a^{21} = \left| \frac{\phi_{ext}^{12} - \phi_1}{\phi_{ext}^{12}} \right| \quad (2.17)$$

$$e_{ext}^{21} = \left| \frac{\phi_1 - \phi_2}{\phi_1} \right| \quad (2.18)$$

Finally, the fine-grid convergence index was calculated using Equation 2.19.

$$GCI_{fine}^{21} = \frac{1.25 e_a^{21}}{r_{21}^p - 1} \quad (2.19)$$

The results of the calculations are presented in Table 2.3. The fine mesh with 26.9 million cells is considered for further analysis and will be used to conduct the final numerical studies. The apparent order of the method, p was found by Equation 2.14.

Table 2.3: Parameters in mesh independence study.

Parameter	Value
N_1, N_2, N_3	$26.9 \times 10^6, 9.7 \times 10^6, 4.3 \times 10^6$
h_1, h_2, h_3	0.08, 0.11, 0.14
r_{21}	1.4
r_{32}	1.3
ϕ_1	1838
ϕ_2	1860
ϕ_3	1897
p	2.1
ϕ_{ext}^{21}	1.8×10^3
e_a^{21}	0.0068 %
e_{ext}^{21}	0.0458 %
GCI_{fine}^{21}	1.4 %

CFD involves discretizations and approximations, and therefore errors and uncertainties are unavoidable. To make sure that numerical results are as accurate as possible, it is necessary to make sure that the right equations are being solved and that they are solved correctly. The simulation results are verified by ensuring that residuals reach a satisfactory convergence criteria and that there is a stable mass flow through the domain. This signifies that the solution is computationally correct. The hydraulic representation of the numerical model will be validated by comparing to PIV measurements on a physical scale model of the sand trap and to ADCP measurements of the prototype[2, 3, 21]. As the flow state is highly stochastic, the velocity distributions will never be identical. However, it is useful to make sure that the jet in the diffuser observed in the PIV measurements also exists in the simulated flow. It is also important to ensure that the simulated velocities are of reasonable magnitudes.

Chapter 3

Results and discussions

The results will mainly focus on how the velocity, vorticity, turbulence, and settling patterns vary between the three distinct models, as these are the key factors that affect sand trap efficiency in this case.

3.1 Sand trap efficiency

The sand trap efficiency of the different models were obtained by creating a time integrated particle mass flow report. This measures the total sediment mass entering the domain through the inlet and exiting through the outlet. The total time of 1000 s was found to be sufficient for all suspended sediments to exit the domain, while remaining sediments are travelling along the bed. In the models with ribs implemented, sediments travelling along the bed are observed to pour into the gaps between ribs. At the end of simulation, not all sediments travelling along the bed have reached the ribs. However, a precedent is set by the sediments that do reach the ribs. These are all seen to pour into the ribs instead of passing over them, indicating that this will also be the case for the remaining sediments. Due to limited computational resources, running the simulations for longer was not feasible. Running the simulations until all sediments are either completely settled or out of the domain, could affect the sand trap efficiencies.

Using the model without upgrades as the base line, the mass of sediments exiting through the outlet is reduced by 24.5 % from 2.5×10^3 to 1.9×10^3 kg by including the ribs. This indicates that the ribs are more effective at capturing and trapping bed load sediments than only the weir. By also adding the v-shaped rakes, the amount of sediments escaping the sand trap is increased by 48.5 % from 2.5×10^3 to 3.7×10^3 kg compared to the model without upgrades. The amount of larger sediments trapped can be assumed to be similar before and after including the rakes, as larger sediments cannot be seen to escape the sand trap in neither particle track

plots. The lack of performance from the model with rakes included can therefore be attributed to the turbulent vortices preventing smaller sediments to settle. This reduces sand trap efficiency. The sand trap efficiency of the different models are listed in Table 3.1.

Table 3.1: Sand trap efficiencies

Model	Sediments injected	Sediments exited	Sand trap efficiency
No upgrades	10^5 kg	2.5×10^3 kg	97.5 %
Ribs	10^5 kg	1.9×10^3 kg	98.1 %
Rakes and ribs	10^5 kg	3.7×10^3 kg	96.3 %

In all simulations, the divide between suspended load and bed load appears to be at around 1 mm in diameter. The majority of sediments escaping the sand trap are smaller than this, while the larger sediments travel along the bed by sliding, saltating or rolling. Models for simulating sediment resuspension were not included in the simulations. The bed load sediments are therefore not observed to be resuspended. It has previously been shown that for classically dimensioned sand traps, sediment resuspension mostly occurs for sediments with grain sizes smaller than 2×10^{-4} m [22]. This is below the range of grain sizes used in the present work. Further analyses could be done with resuspension models included and with smaller grain sizes to investigate the rate of sediment resuspension from the bed load. To further improve the sand trap efficiency, a flow calmer in the shape of horizontal bars, as suggested by Richter, should be tested. Instead of acting as a bluff body and inducing turbulence, this flow calmer could break up turbulence structures and improve settling characteristics for smaller sediments. Smoothing the transition between inlet and diffuser by reducing the inclination of the slope was previously suggested as an option to further increase the settling of smaller sediments[3]. However, it was found that this solution does not significantly improve the jet flow behaviour in the diffuser, thus not improving the settling of small sediments.

3.2 Head losses

The head losses, Δh_L , of the different models were calculated from the steady state simulations using the pressure drop-based Darcy-Weisbach equation in Equation 2.3. The pressure difference, Δp is calculated between the inlet and outlet faces of the models. Using the head losses in the model with no upgrades as a base value, the increased head losses caused by the upgrades was calculated by finding the difference in head losses between each of the upgraded models and the base value.

Table 3.2: Head loss, Δh_L , is calculated using Equation 2.3. Increased head loss is found by comparing to model with no upgrades.

Model	Δh_L	Increased head loss
No upgrades	0.166 m	-
Ribs	0.169 m	0.003 m (+1.8 %)
Rakes and ribs	0.187 m	0.021 m (+12.7 %)

As presented in Table 3.2, the head losses caused by including just the ribs is 0.003 m, equating to an increase of 1.8 % for the whole sand trap. Combined with the better sand trap efficiency of this model, this speaks for the value of including ribs in the sand trap. The model with both ribs and rakes included sees an increase in head loss of 12.7 % compared to the model with no upgrades. The large head loss and the relatively poor sand trap efficiency of this model makes it possible to conclude that other types of improvements to the sand trap should be pursued instead.

3.3 Model 1: No upgrades

The model with no upgrades represents the sand trap as it stands today, with a diffuser near the inlet and a weir just upstream of the penstock. The simulation results on this model give a baseline to which results from the other models can be compared. In addition, the results on this model will be compared to PIV and ADCP measurements for validation [2, 3]. The velocity contour plot in Figure 3.1 shows the separation occurring at the entrance of the diffuser and the jet forming above it. Large circulation zones develop both in the horizontal and vertical planes at the entrance of the diffuser. These phenomena were obtained in both PIV results and in other experimental results, and validate the simulations in this work. [11, 21]. Field measurements by Almeland et al. showed that the main current follows the center of the diffuser, which can also be seen in the present results [10]. The turbulence, which develops from the separation in the diffuser, is seen to propagate through the sand trap. The turbulence appears to dissipate as the flow reaches the halfway point, before increasing as it crosses the weir and enters the penstock. The slow dissipation of turbulence may be due to the relative smoothness of the tunnel walls. Increasing the wall roughness to closer resemble the rough unlined tunnel walls in the prototype would affect the simulation results. One possibility is that turbulence would dissipate faster because of the increased energy losses. This would lead to improved sediment settling characteristics in the downstream end of the sand trap. Another possibility is that the rough walls may introduce even higher turbulence, disturbing sediment settling.

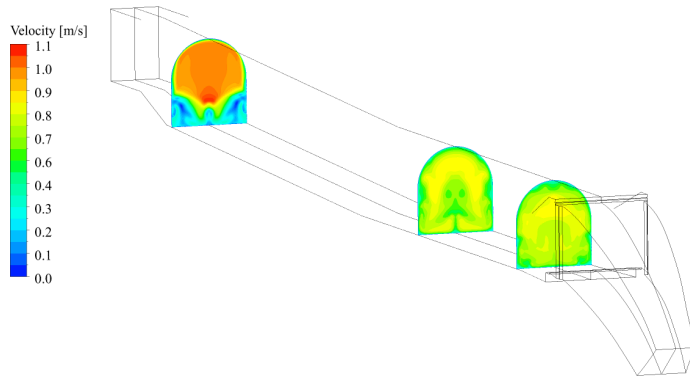


Figure 3.1: Velocity distributions in the sand trap with no upgrades included at $t = 1000$ s. A high velocity jet above vortices caused by flow separation can be seen in the diffuser. Further downstream, the velocity is more evenly distributed.

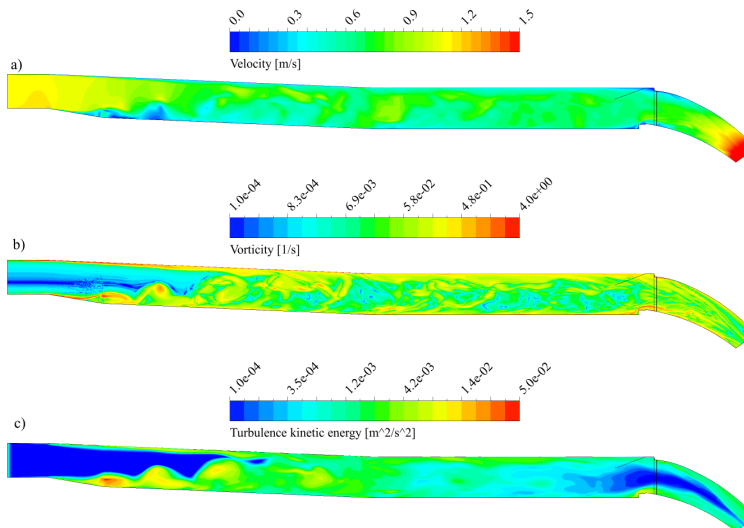


Figure 3.2: Sand trap without upgrades, symmetry plane at $t = 1000$ s. a) Velocity contour. Flow separation occurs in the diffuser which causes a higher flow velocity in the upper part of the diffuser. Separation is also seen to occur at the weir. b) Vorticity contour. Flow separation in the diffuser and at the weir causes vortex generation. c) Turbulence kinetic energy contour. Turbulence propagating from the diffuser starts to dissipate before reaching the penstock.

3.4 Model 2: Sand trap with ribs

The flow behavior upstream of the ribs remains identical to the model without upgrades. Large vortex structures propagate from the diffuser, where flow separation occurs. The separation of the flow field around the ribs is presented in Figure 3.4. This results in low velocities in the space below the ribs, which improves sediment settling. It can also be seen that inflow occurs at the last rib. This causes circulation in the downstream end of the space below the ribs. Sediments begin to settle in the upstream end, and will therefore be less affected by this circulation. However, this could change as the space fills up with sediments. A turbulent boundary layer forms over the ribs from separation at the ramp. This will be beneficial for the settling of bed load sediments under the ribs, as these will slow down when entering this boundary layer. The chance of the sediments falling through the gaps is therefore increased. Flow into the penstock is more turbulent as a consequence of the turbulent boundary layer.

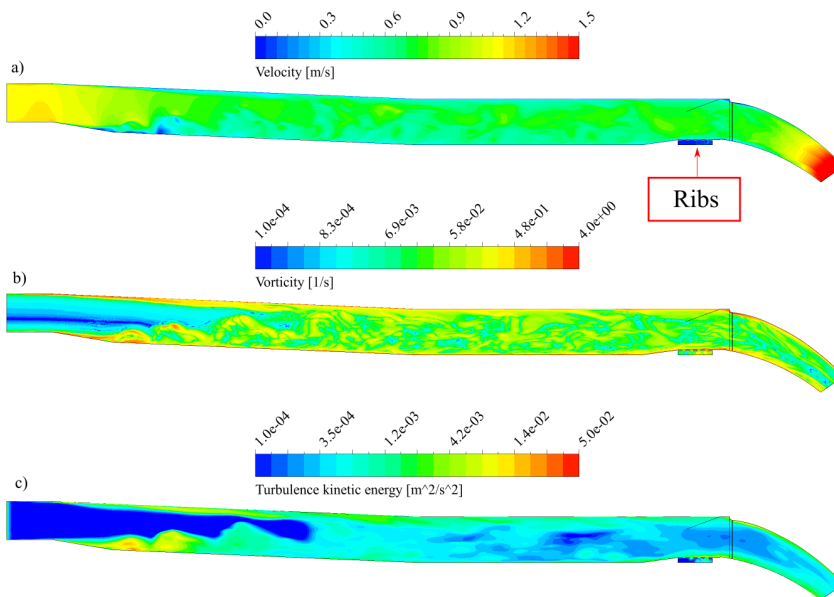


Figure 3.3: View of the sand trap on the symmetry plane at $t = 1000$ s. a) Velocity contour. A separated flow field can be observed over and under the ribs. Flow is identical to the model with no upgrades up until the ramp and ribs. b) Vorticity contour. c) Turbulence kinetic energy contour. Higher turbulence flow is seen to enter the penstock.

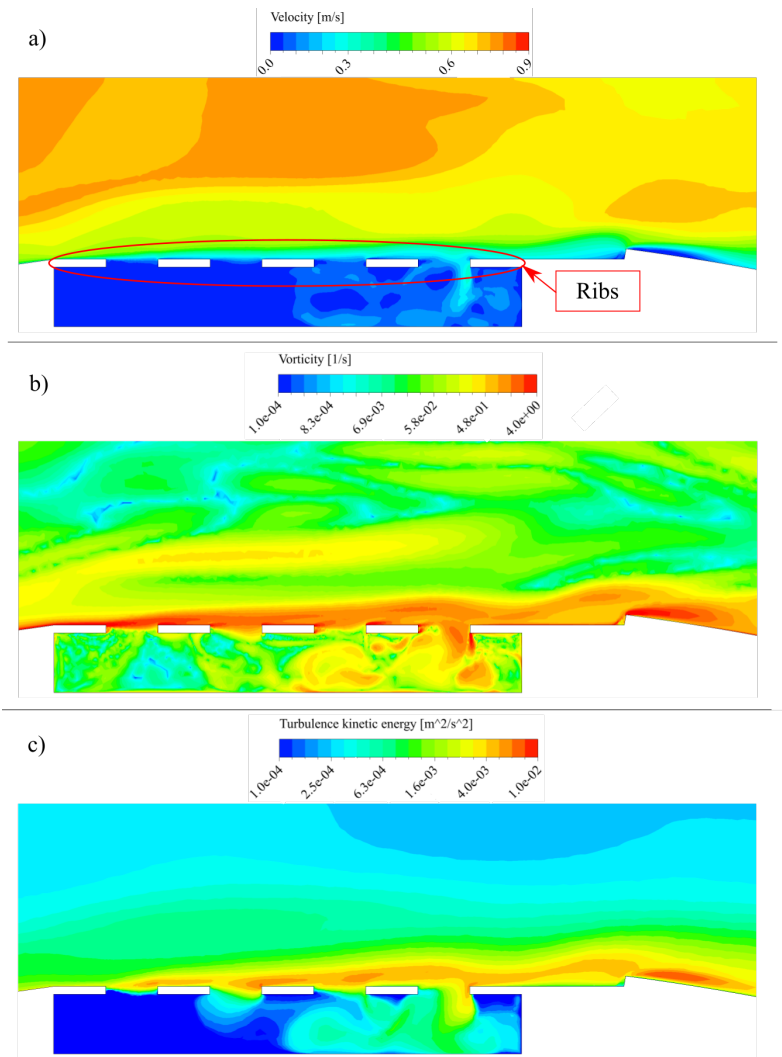


Figure 3.4: Zoomed view of ribs in the symmetry plane at $t = 1000\text{s}$. a) Velocity contour. b) Vorticity contour. c) Turbulence kinetic energy contour.

3.5 Model 3: Sand trap with v-shaped rakes and ribs

It was hypothesised that the higher turbulence induced by the rakes would increase settling speed for larger sediment sizes. By studying the particle tracks in the simulation results, it can be seen that sediments with a diameter larger than 1 mm tend to settle earlier in the sand trap compared to the geometries without the rakes in the diffuser. It can, however, be observed that sediments smaller than 1 mm tend to remain suspended for longer when rakes are included. These smaller sediments have the potential to cause erosion damage on the turbine blades, and it is therefore desired to prevent these from escaping the sand trap.

The large circulation zones, which also occur in the models without rakes, can be seen clearly in Figure 3.6. Sediments are seen to become trapped in these circulation zones in particle track plots. The flow is separated as it passes the rakes, where flow going over is accelerated, while flow going through decelerates and turns turbulent. Vorticity and turbulence is induced by the vortex shedding at the rakes. The highest levels of turbulence are observed between the two rows of rakes. A large turbulent wake is established downstream of the rakes and remains until the outlet. In the present work, this has been shown to decrease sand trap efficiency. The flow downstream of the diffuser when rakes are included is seen to be more turbulent than when rakes are omitted. Because the turbulence does not dissipate before exiting the sand trap, this causes more turbulent flow to enter the penstock.

If the height of the rakes was increased so that they reach the crown of the tunnel, it could affect the settling characteristics in multiple ways. One possibility is that increasing the height of the rakes would cause an earlier onset of turbulence and vorticity, which again carries small diameter sediments further. From the results in the present work, it is believed that this would lead to a decrease in sand trap efficiency. Another possibility is that the flow would no longer be divided into high and low velocity zones downstream of the rakes. Instead, a general reduction in absolute flow velocity would occur. This could mean that the flow becomes more uniform, which might be beneficial for sand trap efficiency. In both cases, increasing the flow obstructing area is likely to increase head losses.

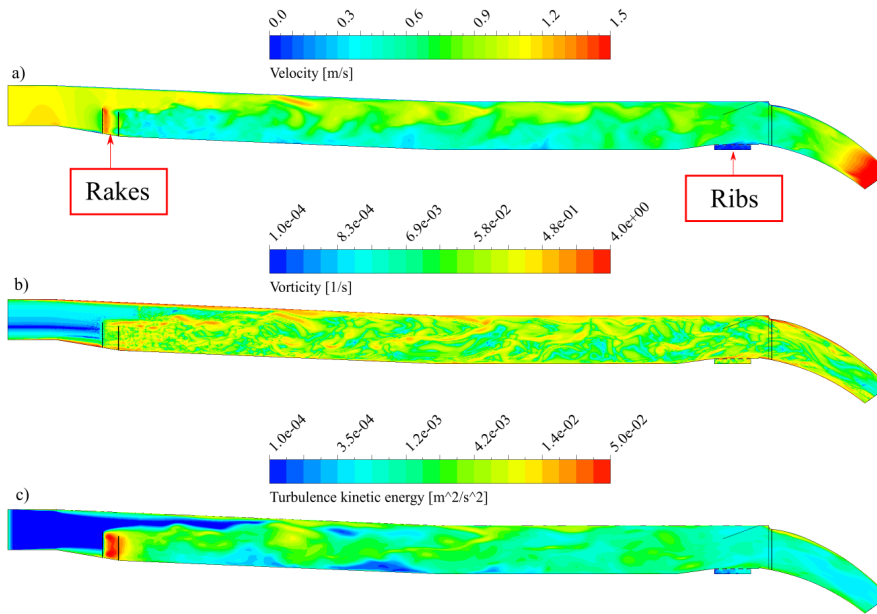


Figure 3.5: Sand trap with ribs and v-shaped rakes, symmetry plane at $t = 1000$ s. a) Velocity contour. Flow over the rakes is accelerated, while flow going through the rakes slows down and turns turbulent. b) Vorticity contour. High vorticity appears immediately downstream of rakes and remains throughout the sand trap. c) Turbulence kinetic energy contour. Rakes induce higher levels of turbulence than can be seen in models without rakes. Turbulence has not dissipated before the flow exits the sand trap.

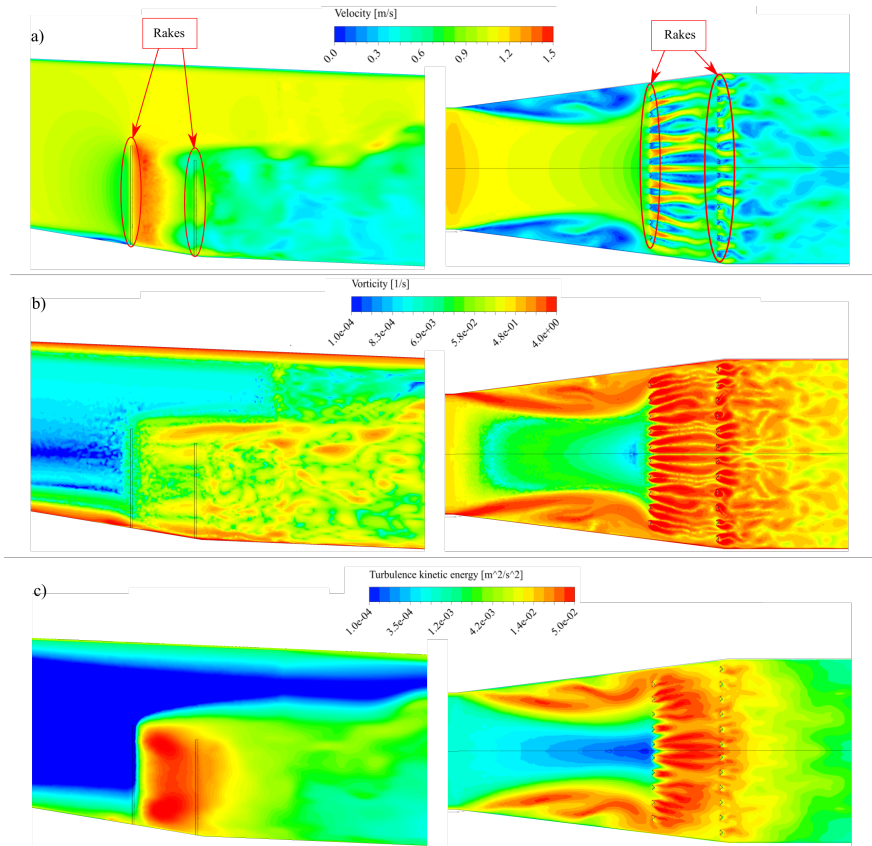


Figure 3.6: Zoomed view of v-shaped rakes in symmetry and horizontal planes at $t = 1000$
 s. a) Velocity contours. b) Vorticity contours. c) Turbulence kinetic energy contours.

3.6 Particle tracks

It is of interest to compare the path of sediments in the best and worst performing sand trap layouts. In the best performing layout, which has ribs near the outlet, the majority of sediments end up travelling as bed load. It appears that particles that reach the tunnel bed before passing over the ribs will fall between them. This confirms what was discovered from experiments by Richter et al.[2, 3]. Sediments that remain suspended when passing the ribs are gathered closer towards the bottom of the tunnel, as presented in Figure 3.7.

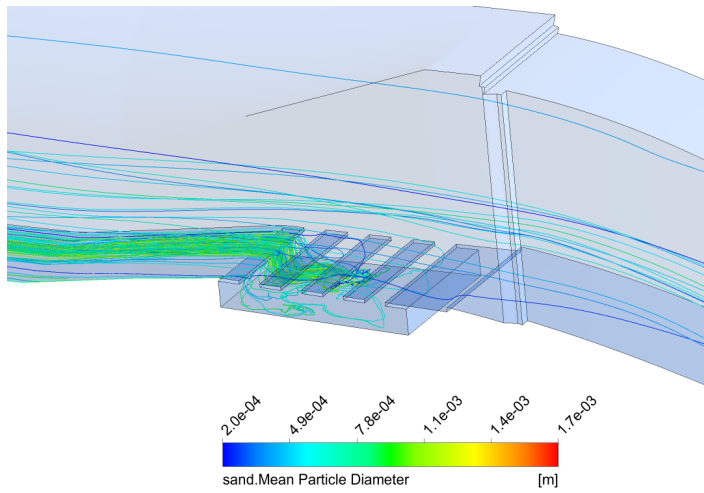


Figure 3.7: Particle track plot at ribs without v-shaped rakes in the diffuser. Only particles smaller than 1 mm remain suspended when reaching the ribs. These are gathered low in the sand trap. Bed load sediments pour between the ribs.

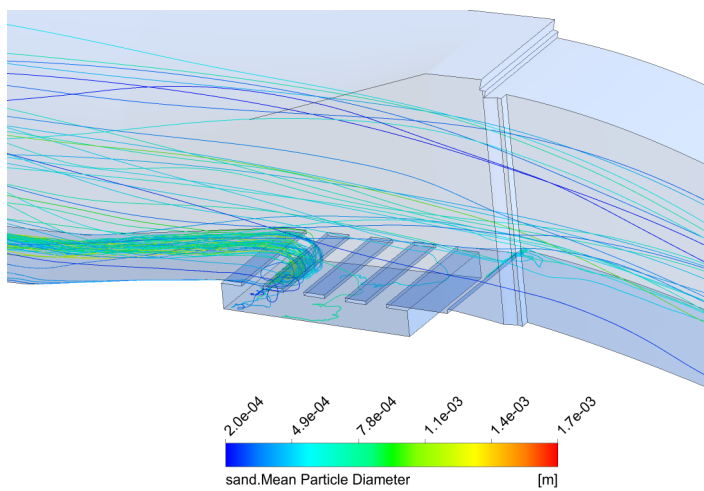


Figure 3.8: Particle track plot at ribs with v-shaped rakes in the diffuser. Sediments are more dispersed over the tunnel cross-section. Larger amounts of sediments are suspended in the flow and pass the ribs.

In the worst performing model, when v-shaped rakes are included in the diffuser, a larger amount of suspended sediments can be seen in Figure 3.8. The sediments are also more dispersed over the tunnel cross-section, instead of gathering closer to the bed. This is believed to be caused by the increased turbulence from the rakes further upstream, which suspends smaller sediments for longer.

Chapter 4

Conclusion

It is necessary to minimize sediment erosion to increase the turbine's life span. In this work, three models based on the Tonstad power plant sand trap were created. One model represents the sand trap as it stands today, while the two others include upgrades to the sand trap to measure their effect on sand trap efficiency and head loss. The first upgrade is a ribbed section installed near the outlet of the sand trap, just upstream of the penstock. This has been shown in physical experiments to increase sand trap efficiency[2]. The other upgrade combines the aforementioned ribs with rows of v-shaped rakes in the diffuser. These rake structures have been shown to increase sediment settling for certain particle sizes in experiments on a physical scale model of the sand trap[12].

This work is part of the FlekS research project, and started with a project report in the fall of 2020. The objective of that project was to use three-dimensional multiphase CFD to investigate the effects on sand trap efficiency by installing rake type structures in the sand trap diffuser. In addition, the project aimed to find the best methods for simulating multiphase flow with a low sediment volume fraction. These methods were applied in the present work. The geometry used in that project work only consisted of the upstream half of the sand trap due to computational limitations. The turbulence patterns in the simulation results matched the areas of sediment settling in experimental work, indicating that the rake structures could improve sediment settling and sand trap efficiency. It was decided that further simulations on the entire sand trap were necessary to reach a conclusion.

In the present work, each of the three models were discretized similarly to each other, with a combination of hexahedral and tetrahedral mesh structures. A mesh independence study was conducted to ensure a reasonably low discretization error. Steady state and transient multiphase simulations were performed on the models, using water and sand with a variable grain size. The one-way coupled fluid pair

model was used to model fluid-solid interactions. The transient simulations were run for 1000 s, where the sediments were injected during the first 100 s.

By investigating the results, it was found that the sand trap with ribs at the outlet reduces total weight of sediments exiting the sand trap by 24.5 % from the base value, while increasing the head loss by 1.8 %. Installing rakes in the diffuser, although showing signs of increasing settling speed for larger sediments, was found to increase the total weight of sediments leaving the sand trap by 48.5 % from the base value. This lead to a reduced sand trap efficiency. In addition, the rakes caused an increased head loss of 12.7 %. It is shown that in all models, sediments escaping the sand trap have a diameter smaller than one millimeter. These findings are supported by physical scale experiments on the sand trap [2, 3, 11]. The results show that installing a ribbed section near the outlet of the sand trap will reduce sediment transport to the turbine and increase sand trap efficiency, thus prolonging turbine life span at Tonstad power plant.

For future work, running two-dimensional simulations along the center line of the sand trap with the Large Eddy Simulation turbulence model could give a more accurate representation of the turbulence and sediment settling in the plane. The effects of extending the rakes so that they reach the crown of the tunnel so that the whole flow area is covered should also be looked at. Additionally, a model allowing for sediment resuspension should be explored for better representation of sediments bouncing on or being resuspended from the bed. Also, experimental measurements of the inlet velocity profile are needed to create realistic and accurate inlet boundary conditions.

References

- [1] Richter, W., Vereide, K., and Zenz, G., 2017, “Upgrading of a Norwegian pressurized sand trap combined with an open air surge tank,” *Geomechanics and Tunnelling*, **10**(5), pp. 620–624, [_eprint: https://onlinelibrary.wiley.com/doi/pdf/10.1002/geot.201700027](https://onlinelibrary.wiley.com/doi/pdf/10.1002/geot.201700027).
- [2] Vereide, K., Richter, W., Havrevoll, O. H., Betete, K., Shrestha, U., Navaratnam, U., Lia, L., and Mauko, G., 2021, “Flexible Sandtraps: Final Report (HydroCen Report; vol. 20),” Tech. rep., Norwegian Research Centre for Hydropower Technology.
- [3] Richter, W., Mauko, G., and Zenz, G., 2020, “Hydraulic Investigation, Numerical and Physical Model Test, Flexible sand trap 2.0,” Tech. rep., Graz University of Technology.
- [4] Maxey, M. R., 1987, “The gravitational settling of aerosol particles in homogeneous turbulence and random flow fields,” *Journal of Fluid Mechanics*, **174**, pp. 441–465, Publisher: Cambridge University Press.
- [5] Wang, L.-P. and Maxey, M. R., 1993, “Settling velocity and concentration distribution of heavy particles in homogeneous isotropic turbulence,” *Journal of Fluid Mechanics*, **256**, pp. 27–68, Publisher: Cambridge University Press.
- [6] Aliseda, A., Cartellier, A., Hainaux, F., and Lasheras, J. C., 2002, “Effect of preferential concentration on the settling velocity of heavy particles in homogeneous isotropic turbulence,” *Journal of Fluid Mechanics*, **468**, pp. 77–105, Publisher: Cambridge University Press.
- [7] Olsen, N. R. B. and Skoglund, M., 1994, “Three-dimensional numerical modeling of water and sediment flow in a sand trap,” *Journal of Hydraulic*

- Research, **32**(6), pp. 833–844, Publisher: Taylor & Francis _eprint: <https://doi.org/10.1080/00221689409498693>.
- [8] Olsen, N. R. B. and Kjellesvig, H. M., 1999, “Three-dimensional numerical modelling of bed changes in a sand trap,” *Journal of Hydraulic Research*, **37**(2), pp. 189–198, Publisher: Taylor & Francis _eprint: <https://doi.org/10.1080/00221689909498305>.
- [9] Bråtteit, K. and Olsen, N. R. B., 2015, “Calibration of Horizontal Acoustic Doppler Current profilers by three dimensional CFD simulations,” *Engineering Applications of Computational Fluid Mechanics*, **9**(1), pp. 41–49.
- [10] Almeland, S. K., Olsen, N. R. B., Bråtteit, K., and Aryal, P. R., 2019, “Multiple solutions of the Navier-Stokes equations computing water flow in sand traps,” *Engineering Applications of Computational Fluid Mechanics*, **13**(1), pp. 199–219, Publisher: Taylor & Francis _eprint: <https://doi.org/10.1080/19942060.2019.1566094>.
- [11] Havrevoll, O. H., Vereide, K., R  ther, N., and Lia, L., “PIV experiments on ribs in the Tonstad rock trap model,” , p. 18.
- [12] Daxnerov  , J., 2019, “Hydraulic Scale Modelling of Flow Calming Structures for Hydropower Plants,” Master’s thesis, NTNU, Trondheim.
- [13] Fergus, T., Hoseth, K. A., and S  terb  , E., 2010, *Vassdragsh  ndboka*, 1st ed., Fagbokforlaget, Trondheim.
- [14] Corson, D., Jaiman, R., and Shakib, F., “Industrial application of RANS modelling: capabilities and needs,” , p. 12.
- [15] Launder, B. E. and Spalding, D. B., 1974, “The numerical computation of turbulent flows,” *Computer Methods in Applied Mechanics and Engineering*, **3**(2), pp. 269–289.
- [16] Menter, F. R., 1994, “Two-equation eddy-viscosity turbulence models for engineering applications,” *AIAA Journal*, **32**(8), pp. 1598–1605, Publisher: American Institute of Aeronautics and Astronautics.
- [17] Menter, F. R. and Egorov, Y., 2010, “The Scale-Adaptive Simulation Method for Unsteady Turbulent Flow Predictions. Part I: Theory and Model Description,” *Flow, Turbulence and Combustion*, **85**(1), pp. 113–138.
- [18] Davidson, L., 2007, “The SAS model: A turbulence model with controlled modelled dissipation,” *20th Nordic Seminar on Computational Mechanics*, 20-23 Nov 2007, G  teborg.

-
- [19] Roache, P. J., 1994, "Perspective: A Method for Uniform Reporting of Grid Refinement Studies," *Journal of Fluids Engineering*, **116**(3), pp. 405–413.
- [20] Celik, I. B. and et al., 2008, "Procedure for Estimation and Reporting of Uncertainty Due to Discretization in CFD Applications," *Journal of Fluids Engineering*, **130**(078001).
- [21] Brevik, O., 2013, "3D numerisk modellering av deler av vannvegen til Tonstad kraftverk," *139*, Accepted: 2014-12-19T11:31:58Z Publisher: Institutt for vann- og miljøteknikk.
- [22] Ortmanns, C., "Ortmanns 2006 Entsander von Wasserkraftanlagen," accessed 2021-06-01, https://docs.google.com/document/d/12pwMDrcKlm5HmpkgiBWZqf8oIZk6oK3uim1jjQMNDk/edit?usp=drive_web&oid=109989660419171606536&usp=embed_facebook

Appendix

Appendix – A

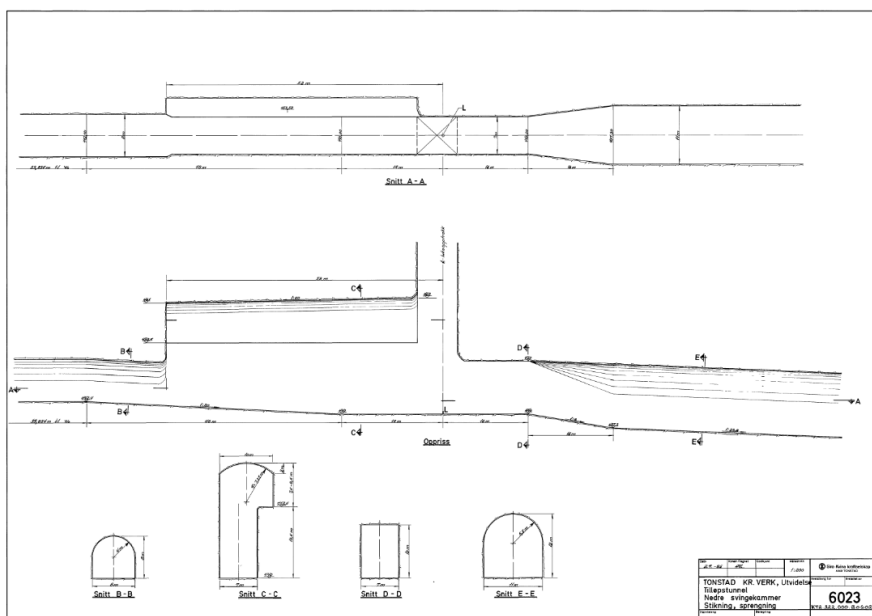


Figure A.1: Engineering drawing of the Tonstad power plant sand trap.[Ref: Sira-Kvina kraftselskap, (2020)]

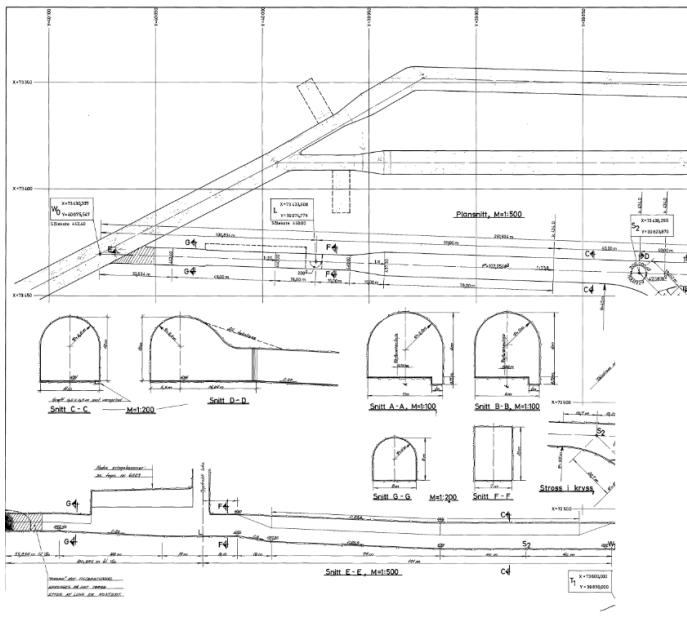


Figure A.2: Engineering drawing of the Tonstad power plant sand trap. Parts of the drawing has been removed, by Sira-Kvina's request.[Ref: Sira-Kvina kraftselskap, (2020)]

Investigations of rake and rib type structures in sand traps to prevent sediment transport in hydropower plants

Mads Mehus Ivarson ¹ Chirag Trivedi ^{1,*}  and Kaspar Vereide ^{2,3}

¹ Waterpower Laboratory, NTNU—Norwegian University of Science and Technology, Alfred Getz' vei 4, 7034 Trondheim, Norway.

² Department of Civil and Environmental Engineering, NTNU—Norwegian University of Science and Technology, 7031 Trondheim, Norway.

³ Sira-Kvina kraftselskap, Stronda 12, 4440 Tonstad, Norway.

* Correspondence: chirag.trivedi@ntnu.no

Abstract: In order to increase the life span of hydraulic turbines in hydropower plants, it is necessary to minimize damages caused by sediment erosion. One solution is to reduce the amount of sediments by improving the sand trap. In the present work, the effects on sand trap efficiency by installing v-shaped rake structures for flow distribution and rib structures for sediment trapping is investigated numerically using the SAS-SST turbulence model. The v-shaped rake structures are located in the diffuser near the inlet of the sand trap, while the ribs cover a section of the bed in the downstream end. Three-dimensional models of the sand trap in Tonstad hydropower plant are created. The present study showed that including ribs reduces the total weight of sediments escaping the sand trap by 24.5 %, which leads to an improved sand trap efficiency. Consequently, the head loss in the sand trap is increased by 1.8 %. By including the v-shaped rakes in addition, the total weight of sediments escaping the sand trap is instead increased by 48.5 %, thus worsening the sand trap efficiency. This increases head loss by 12.7 %. The results also show that turbulent flow commencing at the sand trap diffuser prevents the downstream settling of sediments with a diameter of < 1 mm. The hydraulic representation of the numerical model is validated by comparing to PIV measurements of the flow field from scale experiments and ADCP measurements from the prototype.

Keywords: Hydropower; CFD; sand trap; sediment transport; particle; multiphase

Citation: Ivarson, M. M. Title. *Energies* **2021**, *1*, 0. <https://doi.org/>

Received:

Accepted:

Published:

Publisher's Note: MDPI stays neutral with regard to jurisdictional claims in published maps and institutional affiliations.

Copyright: © 2021 by the authors. Submitted to *Energies* for possible open access publication under the terms and conditions of the Creative Commons Attribution (CC BY) license (<https://creativecommons.org/licenses/by/4.0/>).

1. Introduction

Sediment handling and erosion in hydropower plants are long-standing engineering challenges. Hydropower plants are often upgraded and refurbished to improve performance and plant capacity. After upgrading their installed capacity, several large Norwegian hydropower plants have experienced operational problems associated with sediments entering the penstock and causing erosion to the turbine [1]. Moreover, a higher variability in power demand in recent years has led to some plants converting from base-load to peak-load production. This results in variable discharge through the tunnels, which stirs up sediments from the tunnel bed in unlined tunnels with remaining rock material on the invert, which is typical in Norwegian hydropower plants.

Tonstad hydropower plant, located in the mountains of south-western Norway, is currently experiencing such challenges. In 1988, the plant upgraded its capacity from 640 to 960 MW by installing a new 320 MW Francis turbine. An additional penstock, surge tank, and sand trap was built. However, the unlined headrace tunnel was left untouched. It was expected that the higher discharge required to run all three turbines would lead to an increased amount of sand and rocks to be flushed into the turbines. However, the actual amount of sediments being transported with the flow was surprisingly large. One of the reasons for the increased amount of sediment transport is the poor design of the sand trap, which was designed in the 1960s, and is now under-performing.

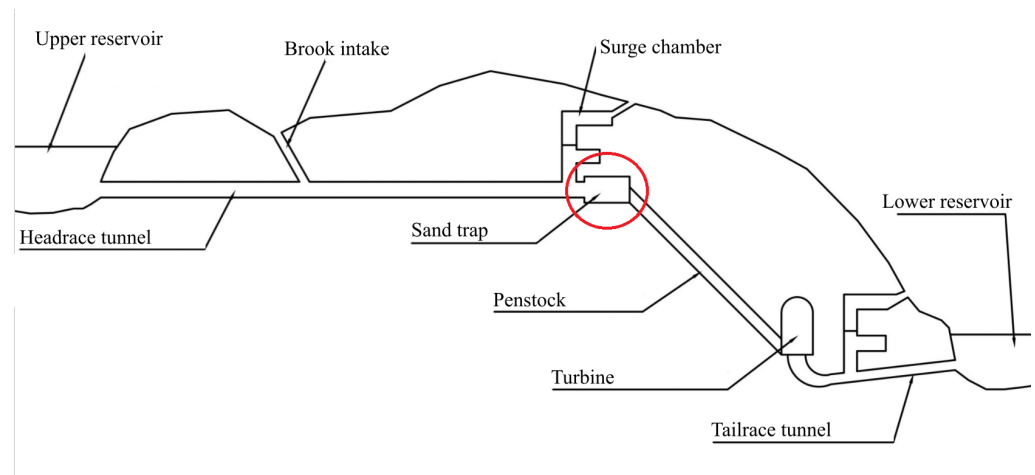


Figure 1. Layout of a typical high-head hydropower plant. The sand trap is circled in red.

37 **Figure 1** shows the layout of a typical high-head hydropower plant. A sand trap is
 38 a section of the water way, typically located immediately upstream of the penstock. This
 39 allows the headrace tunnel, with remaining stone and sand material after its construction,
 40 to be unlined. Sand traps are designed to reduce flow velocity, which allows sediments to
 41 settle easier. The velocity is typically reduced by 30 to 50 % [1]. This is done by increasing
 42 the cross-sectional area of the tunnel. The main challenge is the poor performance of sand
 43 trap, which is supposed to trap sediments before they reach the penstock. A proposal to
 44 improve sand trap performance is to cover sections of the bed with concrete ribs. This
 45 has been shown in physical experiments to create a low velocity zone beneath the ribs,
 46 protecting sediments on the bed from being stirred up, while also allowing sediments to
 47 fall through the gaps between ribs[2,3]. Another proposal is to install rows of v-shaped
 48 rakes in the diffuser at the sand trap inlet. Increased levels of turbulence, such as those
 49 induced by these v-shaped rakes, has been shown to increase sediment settling speeds
 50 for certain particle sizes in numerical studies by Maxey in 1987 [4] and Wang & Maxey
 51 in 1993 [5]. This was later confirmed in physical experiments by Aliseda et al. in 2002
 52 [6]. In these studies, sediments were found to settle in the peripheries of local vortex
 53 structures, which is coupled to a sweeping of sediments in directions normal to the flow.

54
 55 Several scientific studies have been conducted on the topic of sediment transport in
 56 hydropower sand traps. Olsen & Skoglund modelled the flow of water and sediment in
 57 a three-dimensional sand trap geometry using the $k - \epsilon$ turbulence model [7]. After in-
 58 cluding modifications to the turbulence model, both the flow field solution and sediment
 59 concentration calculations were in agreement with experimental procedures. Kjellesvig
 60 & Olsen modelled the bed changes in a sand trap using the transient convection-diffusion
 61 equation for sediment concentration and an adaptive grid adjusting for changes in the
 62 bed [8]. Large amounts of sediments could be seen being moved through the geometry
 63 in the simulations. The results compared well to physical model tests. Bråtveit & Olsen
 64 used 3D computational fluid dynamics (CFD) simulations to calibrate horizontal acoustic
 65 Doppler current profilers (H-ADCP) in the Tonstad sand trap [9]. The study found that
 66 the 3D CFD simulations could accurately calibrate the H-ADCP, while also assessing the
 67 flow conditions at the locations of installation. Almeland et al. computed water flow in
 68 a model of the Tonstad sand trap using different versions of the $k - \epsilon$ turbulence model
 69 [10]. Depending on the discretization scheme, grid resolution and turbulence model, the
 70 computations showed the flow field to follow both the left side, right side and center of
 71 the diffuser. Field measurements showed that the main current follows the center of the
 72 diffuser.

73 The present work is a part of an ongoing sand trap research project. In previous
 74 work by Richter et al., it was found that implementing ribs just upstream of the penstock

75 increased sand trap efficiency dramatically, as sediments were trapped in the low velocity
 76 zone underneath the ribs [2,3]. Havrevoll et al performed PIV analyses on the flow
 77 around ribs in the sand trap to investigate the sediment settling characteristics. They
 78 show that the ribs successfully separate the flow field [11]. Daxnerova performed
 79 experiments on a physical scale model of the sand trap at NTNU to determine the
 80 effects of installing various flow calming structure designs in the diffuser [12]. The best
 81 performing design from Daxnerova's research, a v-shaped rake type structure, will be
 82 further studied in this work.

83 The objectives of the present work is to assess the changes in sand trap efficiency
 84 by including ribs in the downstream end of the sand trap. The effects on the turbulence
 85 dissipation and sediment trajectories by including v-shaped rakes in the diffuser will be
 86 investigated. The work aims to reproduce results from experiments on physical scale
 87 models of the sand trap in order to gain further confidence in the experimental results.

88 2. Numerical analysis

89 2.1. Sediment transport theory

90 When sediments at the tunnel bed are subjected to shear stresses higher than what
 91 is required to loosen them from the bed load, the sediments will be suspended and
 92 transported with the flow. Sediment transport can be divided into two main categories,
 93 depending on the shear velocity to settling velocity ratio of the particles, $u^* > w$ [13].
 94 These categories are *suspended load* and *bed load*. Suspended load consists of finer particles
 95 which have low inertia and settling velocities due to their low mass. They are therefore
 96 transported further by the flow before settling, compared to bed load sediments. The
 97 bed load usually consists of rocks and larger grains of sand which are too heavy to
 98 be suspended in water for longer durations. They are instead transported by sliding,
 99 saltating or rolling along the sediment bed, as illustrated in [Figure 2](#).

100 In order to determine if the upgrades improve sediment settling, it is necessary to
 101 measure the sand trap efficiency. The most straight-forward method to compute the
 102 efficiency is a sediment mass based approach. Here, the ratio of total mass of sediments
 103 injected at the inlet and escaped through the outlet is found. The efficiency can then be
 104 calculated as in [Equation 1](#)

$$\eta = 1 - \frac{\Phi_{s,out}}{\Phi_{s,in}} \quad (1)$$

105 where, η is the sand trap efficiency and Φ represents the mass of sediment. Time
 106 integrated particle mass flow reports created at the end of simulations will be used to
 107 find the inflow and outflow of sediments and then calculate sand trap efficiencies.

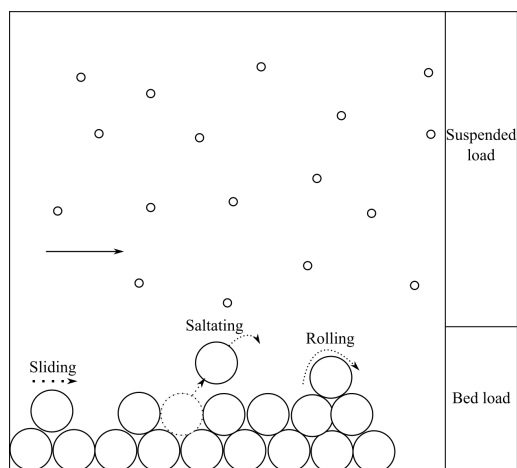


Figure 2. Types of sediment transport.

108 2.2. Head loss

109 Installing new structures in the waterways could increase the energy losses in
110 the flow. This is mainly due to increased friction. This will affect the total head loss
111 and ultimately the performance of the power plant. The head loss should therefore be
112 minimized. Losses due to friction are determined by using the Darcy-Weisbach friction
113 factor, seen in Equation 2.

$$h_f = f \frac{L \times v^2}{D \times 2g} \quad (2)$$

Here, h_f (m) is the head loss, f is the dimensionless Darcy friction factor, L (m) is the length of the pipe, v (m/s) is the mean velocity of the flow, D (m) is the diameter of the tunnel, g (m/s²) is the gravitational acceleration. To ensure correct head loss calculations, it is important to find the correct Darcy friction factor. Using a Moody diagram, the friction factor can be found from knowing the Reynolds number and relative roughness of the flow situation. In the present work, the Darcy-Weisbach equation form based on the pressure drop (Equation 3) will be used to find the head loss caused by the upgrades.

$$\Delta h_L = \frac{\Delta p}{\rho g} \quad (3)$$

114 Here, Δh_L is the head loss, Δp (Pa) is the pressure difference between two points, and ρ
115 (kg/m³) is the fluid density. The head loss in each of the geometries will be measured in
116 post-processing. The head loss in the base case will be subtracted from each of the other
117 cases, where the difference is the increased head loss caused by the upgrades.

118 2.3. Turbulence modelling

119 To model the turbulent flow behaviour in the present work, the scale-adaptive
120 simulation shear stress transport (SAS-SST) turbulence model was used. The model
121 was found to perform better than the conventional RANS formulations in similar cases
122 during the under-lying project work. It introduces the von Karman length scale into the
123 turbulence scale equation to adapt to different turbulence structure sizes, while using
124 base RANS equations in areas where the flow behaves more similar to steady state [14].
125 The SAS-SST are as follows.

$$\frac{\partial k}{\partial t} + \frac{\partial u_j k}{\partial x_j} = P_k - \beta^* \omega k + \frac{\partial}{\partial x_j} \left[\left(\nu + \frac{\nu_t}{\sigma_k} \right) \frac{\partial k}{\partial x_j} \right] \quad (4)$$

$$\frac{\partial \omega}{\partial t} + \frac{\partial}{\partial x_j} (\bar{u}_j \omega) = \frac{\partial}{\partial x_j} \left[\left(\nu + \frac{\nu_t}{\sigma_\omega} \right) \frac{\partial \omega}{\partial x_j} \right] - \beta \omega^2 + C_\omega + \alpha S^2 (1 + P_{SAS}) \quad (5)$$

$$\nu_t \propto \frac{k}{\omega}, \quad P_{SAS} = \bar{\zeta}_2 \kappa \frac{L}{L_{vK,3D}}, \quad L_{vK,3D} = \kappa \frac{S}{U''} \quad (6)$$

126 In these equations, S and U'' are generic first and second velocity derivatives,
127 respectively. The SAS-SST model builds on the SST k-omega model by implementing
128 an extra production term in the ω -equation, P_{SAS} . This term is attuned to transient
129 fluctuations in the flow. In regions with a fine mesh where the flow is turning unsteady,
130 $L_{vK,3D}$ is reduced, increasing the production term. This will result in a large ω and
131 therefore reduced k and ν_t values. In this way, the unsteadiness is not dampened, but
132 instead it is included as a part of the turbulence that is being resolved, leading to greater
133 accuracy. A reduction of the turbulent viscosity dissipation happens, which makes the
134 momentum equations interpret the flow as transient rather than steady [15].

135 2.4. Computational setup

136 The Tonstad power plant sand trap is 184 m long and the main tunnel has a cross-
137 sectional area of 119 m². A 3D model of the sand trap is developed using engineering
138 CAD software. It was created from engineering drawings provided by Sira-Kvina power
139 company, the owner of the plant, and consists of a rectangular inlet section, a diffuser,
140 a long tunnel section with a gentle slope, and a weir in the invert where the tunnel
141 transitions into the penstock. This model is used as a base to add the upgrades to in two
142 other models. The additional models were created to test the effects of the upgrades,
143 where one model includes only ribs and one includes both ribs and v-shaped rakes.

144 The ribs are placed just upstream of the penstock, in combination with the weir.
145 This setup was tested in experiments [2,3]. The purpose of the ribs is to allow bed load
146 sediments to fall between the ribs, while water is minimally affected. There are five
147 ribs in total. The length of the ribs and the gap between ribs are both 1 m. A ramp is
148 placed upstream of the ribs to raise them above the bed and create space for sediments
149 to accumulate. Also, in this way, excavating into the tunnel floor is not necessary. In the
150 work by Richter et al., the ramp was also found to protect the sediments that had fallen
151 between the ribs from being resuspended and flushed into the penstock.

152 The rake structure is made up of two rows of v-shaped rakes, with the tip of the
153 rakes facing downstream. The rakes measure 6 m in height. Distances between rakes
154 are 1 m and 0.8 m for the upstream and downstream row, respectively. The purpose of
155 the rakes is to even the flow of the jet from the inlet and enhance the diffuser effect of
156 slowing down the flow. The distance from the inlet to the rakes is 25 meters, which is
157 approximately 3 times the diameter. To ensure that stable and developed flow reaches
158 the rakes, a distance of 5-10 times the inlet diameter is necessary. The fact that the flow
159 reaching the rakes may not be fully developed in the simulations should be taken into
160 consideration when analysing the results.

161 The three models of the sand trap are meshed similarly. In all three models, the
162 diffuser and the invert are both given tetrahedral mesh structures, while the simpler
163 geometries of the inlet section, tunnel and penstock have structured hexahedral meshes.
164 The number of cells in each mesh is $> 23 \times 10^6$. Inflation layers are added along the tunnel
165 walls so that global $Y^+ < 30$. This ensures accurate representation of flow conditions in
166 the boundary layers. The mesh surrounding the ribs and the rakes are refined further to
167 a maximum cell size of 0.01 m.

168 The chosen advection scheme is the High Resolution scheme available in CFX. This
169 scheme is second order accurate in smooth regions and reduces its order of accuracy
170 in regions of high gradients, where unboundedness is a factor. A first order accurate
171 scheme is generally more robust and reaches convergence criteria faster than a second
172 order accurate scheme. However, this comes at the cost of higher numerical diffusion,
173 resulting in a less accurate solution. The transient scheme used is the Second Order
174 Backward Euler scheme.

175 Steady state multiphase simulations are run to create initial conditions for the
176 transient multiphase simulations. The total simulated time for the transient simulations
177 is set to allow sediments enough time to either reach the bed or exit through the outlet.
178 The simulations use a discharge of 80 m³/s, which is the discharge when the power
179 plant is operating at design conditions. The inlet velocity boundary condition represents
180 this mass flow rate. The wall roughness is 10⁻³ m in the numerical model. An overview
181 of solution parameters and boundary conditions is presented in [Table 1](#).

182 Multiphase flow was implemented by enabling the particle transport solid model in
183 CFX, also known as the discrete phase model (DPM). DPM uses the Eulerian-Lagrangian
184 multiphase model to track the paths of individual particles as they travel through the
185 domain. It is well-suited for situations like in the present work, where the volume
186 fraction of the solid phase is low. The one-way coupled fluid-particle model was chosen
187 to solve the fluid-particle interactions. This model is computationally cheaper than the
188 two-way coupled model. As the sediment phase's effect on the fluid phase is negligible

Table 1: Transient simulation solution parameters.

Parameters	Description
Mesh type	Structured hexahedral and unstructured tetrahedral.
Model scale	1:1 to prototype.
Analysis type	Transient: total time of 1000 s, time step of 0.5 s.
Fluid	Incompressible Newtonian fluid, water density and viscosity at 10 C
Boundary conditions	Inlet: uniform velocity of 1.14 m/s. Outlet: total pressure of 0 Pa. Symmetry plane along center line.
Wall roughness	0.001 m.
Multiphase settings	Multiphase model: Discrete phase model/Particle transport solid. Fluid pair model: One-way coupled. Sediment mass flow rate: 1000 kg/s. Sediment particle diameter: $D_{particle} \sim N(0.75 \text{ mm}, 0.25 \text{ mm})$
Solver controls	Advection scheme: High Resolution. Transient scheme: Second Order Backward Euler.
Turbulence model	SAS-SST.
Convergence control	Maximum residuals for pressure, mass-momentum and turbulent parameters $< 10^{-4}$. Coefficient loops: 2-3 iterations.

189 in this case, the one-way coupled model was found to produce satisfactory results. In
 190 the transient multiphase simulations, sediments were injected with uniform distribution
 191 over the inlet during the first 100 s. Mass flow of sediments is set to 1000 kg/s, which
 192 leads to a total mass of sediments injected into the sand trap to be 10^5 kg. The sediments
 193 are tracked as they travel through the model, and the sand trap efficiency is given by the
 194 time integrated mass flow report at the outlet by the end of the simulation. The sediment
 195 diameters have a normal distribution with a mean of 0.75 mm and a standard deviation
 196 of 0.25 mm.

197 By also ensuring that the solution is mesh independent, the accuracy of the results
 198 are further improved. Mesh independence is achieved when a defining value of the sim-
 199 ulation no longer changes significantly. The purpose of a mesh independence study is to
 200 minimize the discretization error from approximating the geometry during the meshing
 201 stage [16]. The model with both rakes and ribs was used for the mesh independence
 202 study. Three different mesh qualities were used. Following the procedure described by
 203 Celik, I. B., et al. [17], an estimation of the discretization error was performed. In the
 204 calculations, N is the number of cells, h is the representative cell size, r is the refinement
 205 factor, ϕ is the pressure drop from inlet to outlet, p is the apparent order of the method,
 206 ϕ_{ext} are the extrapolated values of ϕ , e_a and e_{ext} are the approximate and extrapolated
 207 relative errors, respectively, and GCI_{fine} is the fine-grid convergence index. The mesh
 208 discretization error was found to be 1.4 %. The results of the calculations are presented
 209 in Table 2. The fine mesh with 26.9 million cells is considered for further analysis and
 210 will be used to conduct the final numerical studies.

211 The simulation results are verified by ensuring that residuals reach a satisfactory
 212 convergence criteria and that there is a stable mass flow through the domain. This
 213 signifies that the solution is computationally correct. The hydraulic representation of the
 214 numerical model will be validated by comparing to PIV measurements on a physical
 215 scale model of the sand trap and to ADCP measurements from the prototype sand
 216 trap [2,18]. As the flow state is highly stochastic, the velocity distributions will never be
 217 identical. However, it is useful to make sure that the jet in the diffuser observed in the
 218 PIV measurements also exists in the simulated flow. It is also important to ensure that
 219 the simulated velocities are of reasonable magnitudes.

Table 2: Parameters in mesh independence study.

Parameter	Value
N_1, N_2, N_3	$26.9 \times 10^6, 9.7 \times 10^6, 4.3 \times 10^6$
h_1, h_2, h_3	0.08, 0.11, 0.14
r_{21}	1.4
r_{32}	1.3
ϕ_1	1838
ϕ_2	1860
ϕ_3	1897
p	2.1
ϕ_{ext}^{21}	1.8×10^3
e_a^{21}	0.0068 %
e_{ext}^{21}	0.0458 %
GCI_{fine}^{21}	1.4 %

220 3. Results and discussions

221 The results will mainly focus on how the velocity, vorticity, turbulence, and settling
 222 patterns vary between the three distinct models, as these are the key factors that affect
 223 sand trap efficiency in this case.

224 3.1. Sand trap efficiency

225 The sand trap efficiency of the different models were obtained by creating a time
 226 integrated particle mass flow report. This measures the total sediment mass entering the
 227 domain through the inlet and exiting through the outlet. The total time of 1000 s was
 228 found to be sufficient for all suspended sediments to exit the domain, while remaining
 229 sediments are travelling along the bed. In the models with ribs implemented, sediments
 230 travelling along the bed are observed to pour into the gaps between ribs. At the end of
 231 simulation, not all sediments travelling along the bed have reached the ribs. However,
 232 a precedent is set by the sediments that do reach the ribs. These are all seen to pour
 233 into the the ribs instead of passing over them, indicating that this will also be the case
 234 for the remaining sediments. Due to limited computational resources, running the
 235 simulations for longer was not feasible. Running the simulations until all sediments are
 236 either completely settled or out of the domain, could affect the sand trap efficiencies.

237 Using the model without upgrades as the base line, the mass of sediments exiting
 238 through the outlet is reduced by 24.5 % from 2.5×10^3 to 1.9×10^3 kg by including the
 239 ribs. This indicates that the ribs are more effective at capturing and trapping bed
 240 load sediments than only the weir. By also adding the v-shaped rakes, the amount of
 241 sediments escaping the sand trap is increased by 48.5 % from 2.5×10^3 to 3.7×10^3 kg
 242 compared to the model without upgrades. The amount of larger sediments trapped can
 243 be assumed to be similar before and after including the rakes, as larger sediments cannot
 244 be seen to escape the sand trap in neither particle track plots. The lack of performance
 245 from the model with rakes included can therefore be attributed to the turbulent vortices
 246 preventing smaller sediments to settle. This reduces sand trap efficiency. The sand trap
 247 efficiency of the different models are listed in [Table 3](#).

Table 3: Sand trap efficiencies

Model	Sediments injected	Sediments exited	Sand trap efficiency
No upgrades	10^5 kg	2.5×10^3 kg	97.5 %
Ribs	10^5 kg	1.9×10^3 kg	98.1 %
V-shaped rakes and ribs	10^5 kg	3.7×10^3 kg	96.3 %

248 In all simulations, the divide between suspended load and bed load appears to be
 249 at around 1 mm in diameter. The majority of sediments that remain suspended until
 250 escaping the sand trap are smaller than 1 mm, while the larger sediments travel along
 251 the bed by sliding, saltating or rolling. Models for simulating sediment resuspension
 252 was not included in the simulations. The bed load sediments are therefore not observed
 253 to be resuspended. It has previously been shown that for classically dimensioned sand
 254 traps, sediment resuspension mostly occurs for sediments with grain sizes smaller than
 255 2×10^{-4} m [19]. This is below the range of grain sizes used in the present work. Further
 256 analyses could be done with resuspension models included and with smaller grain sizes
 257 to investigate the rate of sediment resuspension from the bed load. To further improve
 258 the sand trap efficiency, a flow calmer in the shape of horizontal bars, as suggested by
 259 Richter, should be tested. Instead of acting as a bluff body and inducing turbulence, this
 260 flow calmer could break up turbulence structures and improve settling characteristics
 261 for smaller sediments. Smoothing the transition between inlet and diffuser by reducing
 262 the inclination of the slope was suggested as an option to further increase the settling of
 263 smaller sediments[3]. However, it was found that this solution does not significantly
 264 improve the jet flow behaviour in the diffuser, thus not improving the settling of small
 265 sediments.

266 Looking at particle track plots of the different models, it appears that particles that
 267 reach the tunnel bed before passing over the ribs will indeed fall between them. This
 268 confirms what was discovered from experiments by Richter et al.[2,3]. Sediments that
 269 remain suspended when passing the ribs will generally escape the sand trap. The amount
 270 of suspended sediments vary depending on if rakes are included in the diffuser or not.
 271 In the results where the rakes are not included, the suspended sediments are gathered
 272 closer towards the bottom of the tunnel. When rakes are included, the suspended
 273 sediments are of greater numbers and are more dispersed over the tunnel cross-section.
 274 This is believed to be caused by the turbulence from the rakes.

275 3.2. Head losses

276 The head loss, Δh_L , of the different models was calculated from the steady state
 277 simulations using pressure drop-based Darcy-Weisbach equation in Equation 3. The
 278 pressure difference, Δp is calculated between the inlet and outlet faces of the models.
 279 Using the head loss in the model with no upgrades as a base value, the increased
 280 head loss caused by the upgrades was calculated by finding the difference in head loss
 281 between each of the upgraded models and the base value.

Table 4: Head loss, Δh_L , is calculated using Equation 3. Increased head loss is found by comparing to model with no upgrades.

Model	Δh_L	Increased head loss
No upgrades	0.166 m	-
Ribs	0.169 m	0.003 m (+1.8 %)
V-shaped rakes and ribs	0.187 m	0.021 m (+12.7 %)

282 As presented in Table 4, the head loss caused by including just the ribs is 0.003
 283 m, equating to an increase of 1.8 % for the whole sand trap. Combined with the better
 284 sand trap efficiency of this model, this speaks for the value of including ribs in the sand
 285 trap. The model with both ribs and rakes included sees an increase in head loss of 12.7
 286 % compared to the model with no upgrades. The large head loss and the relatively
 287 poor sand trap efficiency of this model makes it possible to conclude that other types of
 288 improvements to the sand trap should be pursued instead.

289 3.3. No upgrades

290 The model with no upgrades represents the sand trap as it stands today, with a
 291 diffuser near the inlet and a weir just upstream of the penstock. The simulation results
 292 on the model with no upgrades give a baseline to which results from the other models

293 can be compared. In addition, the results on this model will be compared to PIV and
294 ADCP measurements for validation [2,3]. The velocity contour plot in Figure 4 shows the
295 separation occurring at the entrance of the diffuser and the jet forming above it. Large
296 circulation zones develop both in the horizontal and vertical planes at the entrance of the
297 diffuser. These phenomena were obtained in both PIV results and in other experimental
298 results, and validate the simulations in this work. [11,18]. Field measurements by
299 Almeland et al. showed that the main current follows the center of the diffuser, which
300 can also be seen in the present results [10].

301 The turbulence, which develops from the separation in the diffuser, is seen to
302 propagate through the sand trap. The turbulence appears to dissipate as the flow reaches
303 the halfway point, before increasing as it crosses the weir and enters the penstock. The
304 slow dissipation of turbulence may be due to the relative smoothness of the tunnel walls.
305 Increasing the wall roughness to closer resemble the rough unlined tunnel walls in the
306 prototype would affect the simulation results. One possibility is that turbulence would
307 dissipate faster because of the increased energy losses. This would lead to improved
308 sediment settling characteristics in the downstream end of the sand trap. Another
309 possibility is that the rough walls may introduce even higher turbulence, disturbing
310 sediment settling.

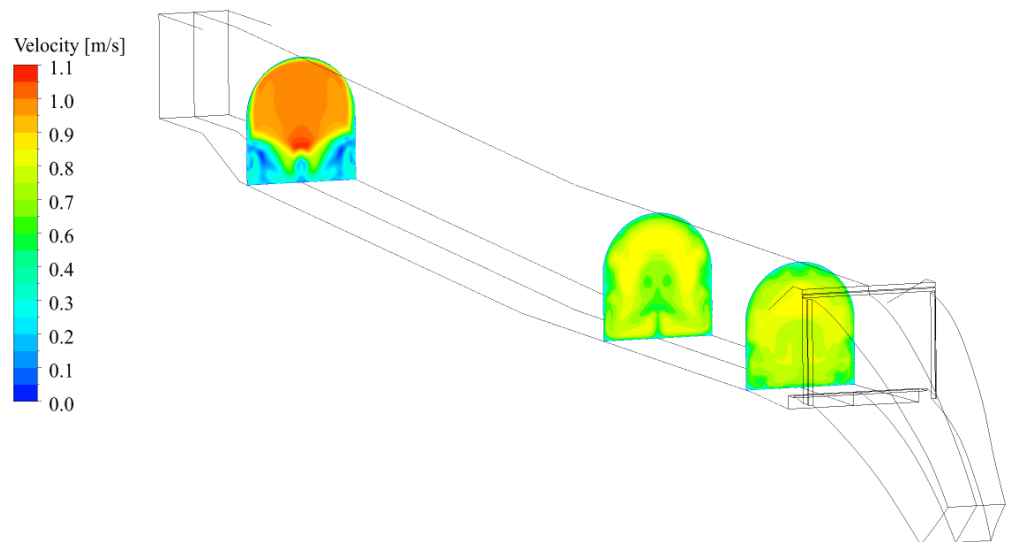


Figure 4. Velocity distributions in the sand trap with no upgrades included at $t = 1000$ s. A high velocity jet above vortices caused by flow separation can be seen in the diffuser. Further downstream, the velocity is more evenly distributed.

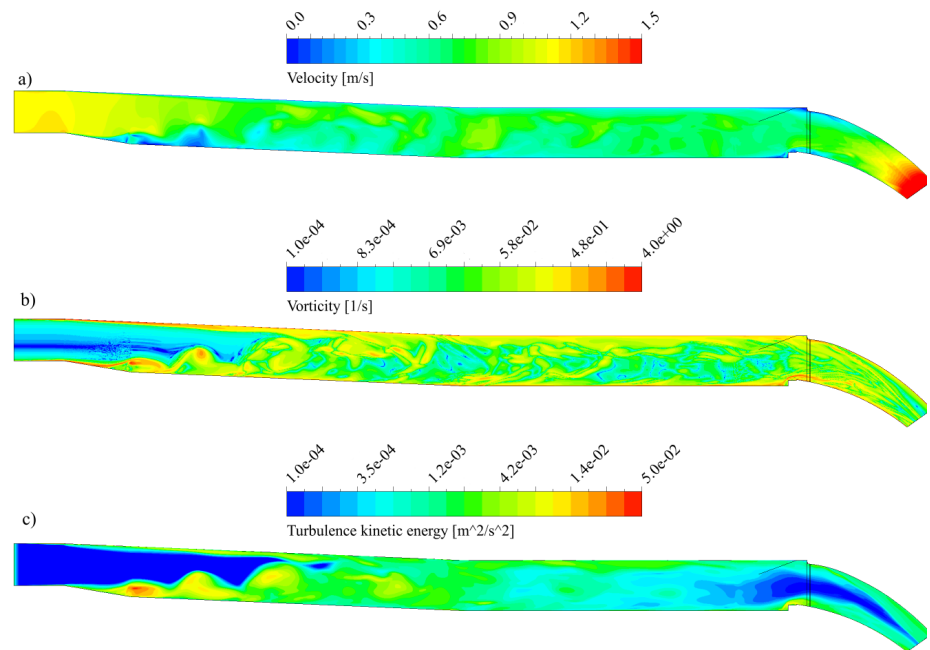


Figure 5. Sand trap without upgrades, symmetry plane at $t = 1000$ s. a) Velocity contour. Flow separation occurs in the diffuser which causes a higher flow velocity in the upper part of the diffuser. Separation is also seen to occur at the weir. b) Vorticity contour. Flow separation in the diffuser and at the weir causes vortex generation. c) Turbulence kinetic energy contour. Turbulence propagating from the diffuser starts to dissipate before reaching the penstock.

311 3.4. Sand trap with ribs

312 The flow behavior upstream of the ribs remains identical to the model without
 313 upgrades. Large vortex structures propagate from the diffuser, where flow separation
 314 occurs. The separation of the flow field around the ribs is presented in Figure 6. This
 315 results in low velocities in the space below the ribs, which improves sediment settling.
 316 It can also be seen that inflow occurs at the last rib. This causes circulation in the
 317 downstream end of the space below the ribs. Sediments begin to settle in the upstream
 318 end, and will therefore be less affected by this circulation. However, this could change
 319 as the space fills up with sediments. A turbulent boundary layer forms over the ribs
 320 from separation at the ramp. This will be beneficial for the settling of bed load sediments
 321 under the ribs, as these will slow down when entering this boundary layer. The chance
 322 of the sediments falling through the gaps is therefore increased. Flow into the penstock
 323 is more turbulent as a consequence of the turbulent boundary layer.

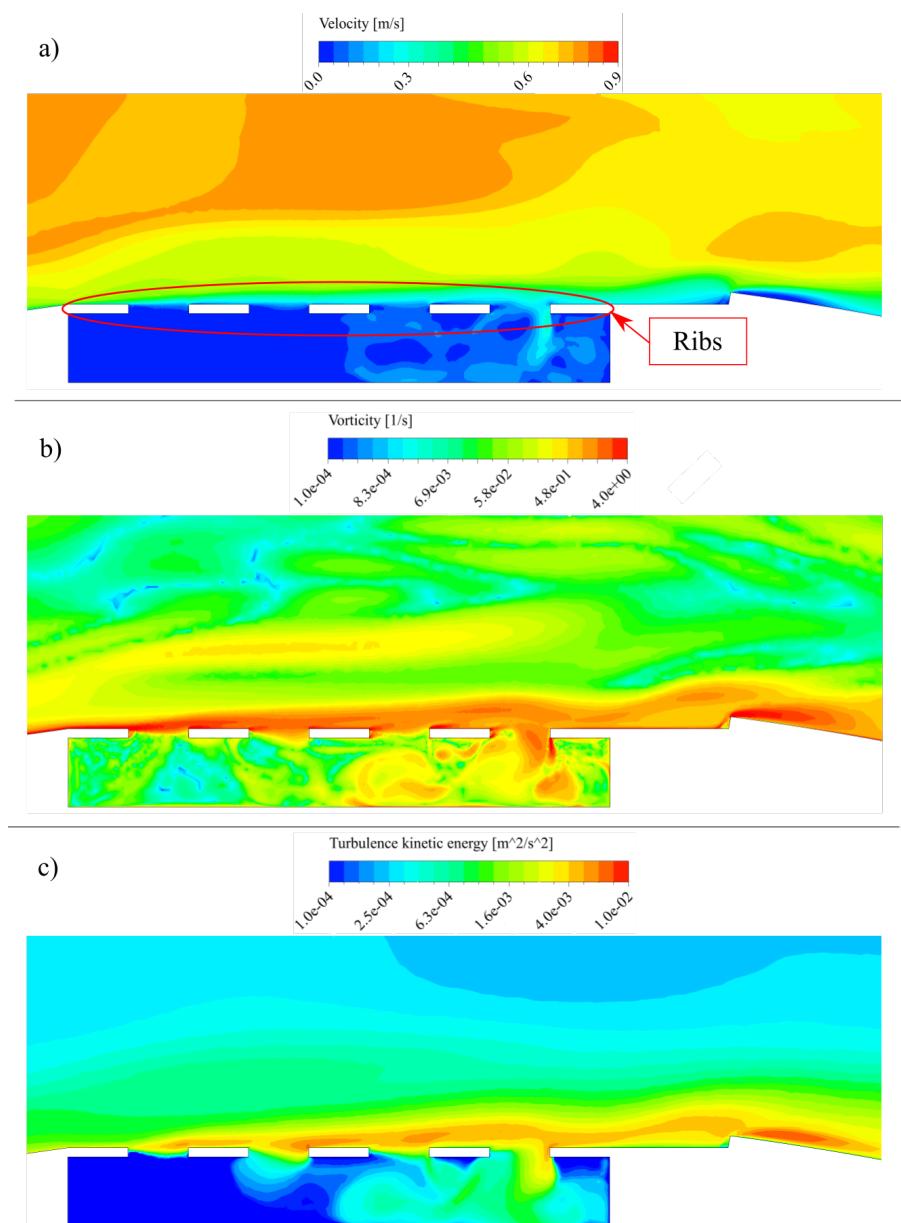


Figure 6. Zoomed view of ribs in the symmetry plane at $t = 1000\text{s}$. a) Velocity contour. Separation of the velocity field is visible. Low velocities below ribs increases the chances of sediment settling. Low velocity inflow occurs between the last two ribs. This causes circulation in the downstream end below the ribs. Sediments will begin to settle in the upstream end, and will therefore be less affected by the circulation. However, this could change as the space fills up with sediments. b) Vorticity contour. c) Turbulence kinetic energy contour. A turbulent boundary layer forms over the ribs from separation from the ramp. This will be beneficial for the settling of bed load sediments, as these will slow down when entering this boundary layer. Flow into the penstock is more turbulent as a consequence.

324 3.5. Sand trap with rakes and ribs

325 It was hypothesised that the higher turbulence induced by the rakes would increase
 326 settling speed for larger sediment sizes. By studying the particle tracks in the simulation
 327 results, it can be seen that sediments with a diameter larger than 1 mm tend to settle
 328 earlier in the sand trap compared to the geometries without the rakes in the diffuser. It
 329 can, however, be observed that sediments smaller than 1 mm tend to remain suspended
 330 for longer when rakes are included. These smaller sediments have the potential to cause

331 erosion damage on the turbine blades, and it is therefore desired to prevent these from
 332 escaping the sand trap. .

333 The large circulation zones, which also occur in the models without rakes, can
 334 be seen clearly in Figure 8. Sediments are seen to become trapped in these circulation
 335 zones in particle track plots. The flow is separated as it passes the rakes, where flow
 336 going over is accelerated, while flow going through decelerates and turns turbulent.
 337 Vorticity and turbulence is induced by the vortex shedding at the rakes. The highest
 338 levels of turbulence are observed between the two rows of rakes. A large turbulent
 339 wake is established downstream of the rakes and remains until the outlet. In the present
 340 work, this has been shown to decrease sand trap efficiency. The flow downstream of
 341 the diffuser when rakes are included is seen to be more turbulent than when rakes are
 342 omitted. Because the turbulence does not dissipate before exiting the sand trap, this
 343 causes more turbulent flow to enter the penstock.

344 If the height of the rakes was increased so that they reach the crown of the tunnel, it
 345 could affect the settling characteristics in multiple ways. One possibility is that increasing
 346 the height of the rakes would cause an earlier onset of turbulence and vorticity, which
 347 again carries small diameter sediments further. From the results in the present work, it
 348 is believed that this would lead to an increase in head loss and a decrease in sand trap
 349 efficiency. Another possibility is that the flow would no longer be divided into high and
 350 low velocity zones downstream of the rakes. Instead, a general reduction in absolute
 351 flow velocity would occur. This could mean that the flow becomes more uniform, which
 352 might be beneficial for sand trap efficiency. In both cases, increasing the flow obstructing
 353 area is likely to increase head loss.

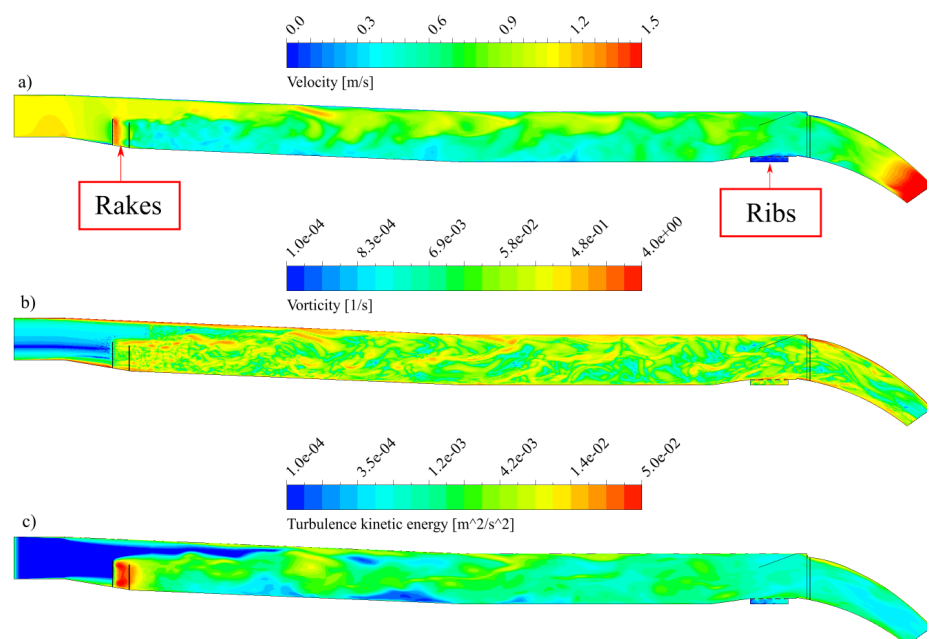


Figure 7. Sand trap with ribs and v-shaped rakes, symmetry plane at $t = 1000$ s. a) Velocity contour. Flow over the rakes is accelerated, while flow going through the rakes slows down and turns turbulent. b) Vorticity contour. High vorticity appears immediately downstream of rakes and remains throughout the sand trap. c) Turbulence kinetic energy contour. Rakes induce higher levels of turbulence than can be seen in models without rakes. Turbulence has not dissipated before the flow exits the sand trap

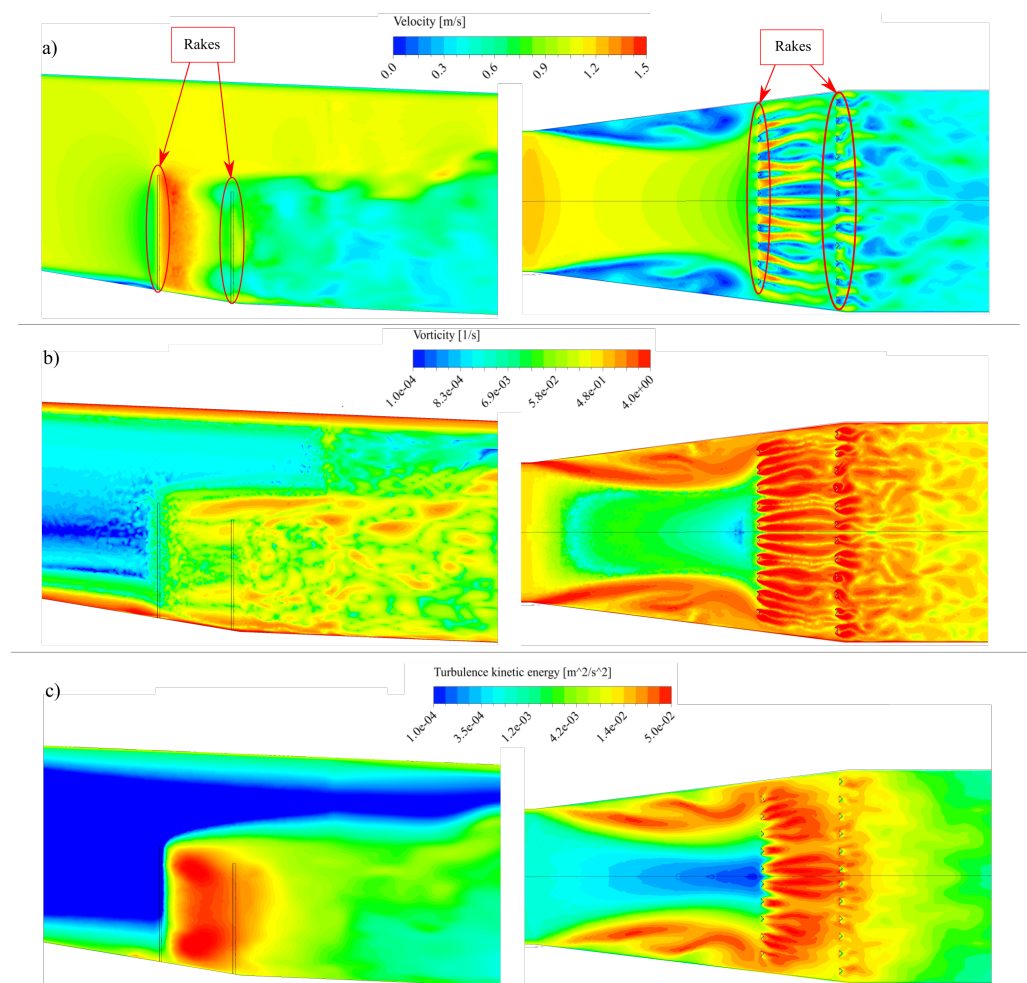


Figure 8. Zoomed view of v-shaped rakes in symmetry and horizontal planes at $t = 1000$ s. a) Velocity contours. The large circulation zones which can also be seen in the models without rakes, appear at the entrance of the diffuser. These zone are seen trapping sediments. Flow is separated going past the rakes. Flow going over is accelerated, while flow going through is decelerated. Velocity is highest between rakes. b) Vorticity contours. Vorticity and turbulence is induced by the vortex shedding at the rakes. c) Turbulence kinetic energy contours. The highest levels of turbulence are observed between the two rows of rakes. A large turbulent wake is established downstream of the rakes, which in the present work has been shown to decrease sand trap efficiency.

354 4. Conclusions

355 It is necessary to minimize sediment erosion to increase the turbine's span. Three-
 356 dimensional models based on the Tonstad power plant sand trap were created. Versions
 357 of the model include various upgrades to determine their effect on sediment settling.
 358 The geometries was discretized by a combination of hexahedral and tetrahedral mesh.
 359 Steady state and transient multiphase simulations were performed on the models, using
 360 water and sand with a variable grain size. The objective was to investigate how installing
 361 rake or rib type structures affect sand trap efficiency and head loss.

362 By investigating the results, it was found that the sand trap with ribs at the outlet
 363 reduces total weight of sediments exiting the sand trap by 24.5 % while increasing the
 364 head loss around 1.8 %. Installing rakes in the diffuser, although showing signs of
 365 increasing settling speed for larger sediments, was found to increase the total weight of
 366 sediments leaving the sand trap by 48.5 %. This lead to a reduced sand trap efficiency.
 367 In addition, the rakes caused an increased head loss of 12.7 %. It is shown that in all
 368 models, sediments escaping the sand trap have a diameter smaller than one millimeter.

369 These findings are supported by physical scale experiments on the sand trap [2,3,11].
370 The results show that installing ribs at the outlet of the sand trap will reduce sediment
371 transport to the turbine and increase sand trap efficiency, thus prolonging turbine life
372 span at Tonstad power plant.

373 5. Further work

374 For further work, running two-dimensional simulations along the center line of
375 the sand trap with the Large Eddy Simulation turbulence model could give a more
376 accurate representation of the turbulence and sediment settling in the plane. The effects
377 of extending the rakes so that they reach the crown of the tunnel so that the whole flow
378 area is covered should also be looked at. Additionally, model allowing for sediment
379 resuspension should be explored to better represent sediments bouncing on or being
380 resuspended from the bed. Also, experimental measurements of the inlet velocity profile
381 are needed to create realistic and accurate inlet boundary conditions.

382 **Author Contributions:** “Conceptualization, MM.I.; C.T.; and K. V. methodology, MM.I.;
383 software, MM.I.; formal analysis, MM.I.; investigation, MM.I.; resources, C. T.; data
384 curation, MM.I.; writing original draft preparation, MM.I.; writing—review and editing,
385 C.T. and K. V.; visualization, MM.I.; supervision, C. T. and K. V.; project administration,
386 C. T. All authors have read and agreed to the published version of the manuscript.”

387 **Conflicts of Interest:** The authors declare no conflict interest.

388 References

- 389
- 390 1. Richter, W.; Vereide, K.; Zenz, G. Upgrading of a Norwegian pressurized sand trap
391 combined with an open air surge tank. *Geomechanics and Tunneling* **2017**, *10*, 620–
392 624. _eprint: <https://onlinelibrary.wiley.com/doi/pdf/10.1002/geot.201700027>, doi:
393 <https://doi.org/10.1002/geot.201700027>.
 - 394 2. Vereide, K.; Richter, W.; Havrevoll, O.H.; Betete, K.; Shrestha, U.; Navaratnam, U.; Lia, L.;
395 Mauko, G. Flexible Sandtraps: Final Report (HydroCen Report; vol. 20). Technical report,
396 Norwegian Research Centre for Hydropower Technology, 2021.
 - 397 3. Richter, W.; Mauko, G.; Zenz, G. Hydraulic Investigation, Numerical and Physical Model
398 Test, Flexible sand trap 2.0. Technical report, Graz University of Technology, 2020.
 - 399 4. Maxey, M.R. The gravitational settling of aerosol particles in homogeneous turbulence and
400 random flow fields. *Journal of Fluid Mechanics* **1987**, *174*, 441–465. Publisher: Cambridge
401 University Press, doi:10.1017/S0022112087000193.
 - 402 5. Wang, L.P.; Maxey, M.R. Settling velocity and concentration distribution of heavy particles
403 in homogeneous isotropic turbulence. *Journal of Fluid Mechanics* **1993**, *256*, 27–68. Publisher:
404 Cambridge University Press, doi:10.1017/S0022112093002708.
 - 405 6. Aliseda, A.; Cartellier, A.; Hainaux, F.; Lasheras, J.C. Effect of preferential concentration
406 on the settling velocity of heavy particles in homogeneous isotropic turbulence. *Jour-*
407 *nal of Fluid Mechanics* **2002**, *468*, 77–105. Publisher: Cambridge University Press, doi:
408 10.1017/S0022112002001593.
 - 409 7. Olsen, N.R.B.; Skoglund, M. Three-dimensional numerical modeling of water and sediment
410 flow in a sand trap. *Journal of Hydraulic Research* **1994**, *32*, 833–844. Publisher: Taylor & Francis
411 _eprint: <https://doi.org/10.1080/00221689409498693>, doi:10.1080/00221689409498693.
 - 412 8. Olsen, N.R.B.; Kjellesvig, H.M. Three-dimensional numerical modelling of bed changes in a
413 sand trap. *Journal of Hydraulic Research* **1999**, *37*, 189–198. Publisher: Taylor & Francis _eprint:
414 <https://doi.org/10.1080/00221689909498305>, doi:10.1080/00221689909498305.
 - 415 9. Bråtveit, K.; Olsen, N.R.B. Calibration of Horizontal Acoustic Doppler Current profilers by
416 three dimensional CFD simulations. *Engineering Applications of Computational Fluid Mechanics*
417 **2015**, *9*, 41–49. doi:10.1080/19942060.2015.1004807.
 - 418 10. Almeland, S.K.; Olsen, N.R.B.; Bråveit, K.; Aryal, P.R. Multiple solutions of the Navier-
419 Stokes equations computing water flow in sand traps. *Engineering Applications of*
420 *Computational Fluid Mechanics* **2019**, *13*, 199–219. Publisher: Taylor & Francis _eprint:
421 <https://doi.org/10.1080/19942060.2019.1566094>, doi:10.1080/19942060.2019.1566094.
 - 422 11. Havrevoll, O.H.; Vereide, K.; Rütther, N.; Lia, L. PIV experiments on ribs in the Tonstad rock
423 trap model. p. 18.

-
- 424 12. Daxnerová, J. Hydraulic Scale Modelling of Flow Calming Structures for Hydropower Plants.
425 Master's thesis, NTNU, Trondheim, 2019.
- 426 13. Fergus, T.; Hoseth, K.A.; Sæterbø, E. *Vassdragshåndboka*, 1 ed.; Fagbokforlaget: Trondheim,
427 2010.
- 428 14. Menter, F.R.; Egorov, Y. The Scale-Adaptive Simulation Method for Unsteady Turbulent Flow
429 Predictions. Part 1: Theory and Model Description. *Flow, Turbulence and Combustion* **2010**,
430 *85*, 113–138. doi:10.1007/s10494-010-9264-5.
- 431 15. Davidson, L. The SAS model: A turbulence model with controlled modelled dissipation.
432 *20th Nordic Seminar on Computational Mechanics, 20-23 Nov 2007, Göteborg* **2007**.
- 433 16. Roache, P.J. Perspective: A Method for Uniform Reporting of Grid Refinement Studies.
434 *Journal of Fluids Engineering* **1994**, *116*, 405–413. doi:10.1115/1.2910291.
- 435 17. Celik, I.B.; et al.. Procedure for Estimation and Reporting of Uncertainty Due to Discretization
436 in CFD Applications. *Journal of Fluids Engineering* **2008**, *130*. doi:10.1115/1.2960953.
- 437 18. Brevik, O. 3D numerisk modellering av deler av vannvegen til Tonstad kraftverk. *139* **2013**.
438 Accepted: 2014-12-19T11:31:58Z Publisher: Institutt for vann- og miljøteknikk.
- 439 19. Ortmanns, C. Ortmanns 2006 Entsander von Wasserkraftanlagen.

